THESIS FOR THE DEGREE OF DOCTOR OF PHILOSOPHY IN APPLIED ACOUSTICS

A refined ground-borne noise prediction methodology for railway traffic in tunnels in bedrock

Fatemeh Dashti

Department of Architecture And Civil Engineering
Division of Applied Acoustics
CHALMERS UNIVERSITY OF TECHNOLOGY
Gothenburg, Sweden, 2025

A refined ground-borne noise prediction methodology for railway traffic in tunnels in bedrock

Fatemeh Dashti
ISBN: 978-91-8103-262-8

Doktorsavhandlingar vid Chalmers tekniska högskola
Ny serie nr 5720
ISSN 0346-718X

Department of Architecture And Civil Engineering
Chalmers University of Technology
SE-412 96 Gothenburg, Sweden
Telephone: +46 (0)31 772 1000

Cover: Measured vibration signal from a train passage, recorded on a sleeper inside the Gårda tunnel during field tests.

Printed by Chalmers Reproservice
Gothenburg, Sweden, 2025

A refined ground-borne noise prediction methodology for railway traffic in tunnels in bedrock

Fatemeh Dashti
Department of Architecture And Civil Engineering
Chalmers University of Technology

ABSTRACT

The expansion of railway networks has significantly improved transportation efficiency but has also led to increased noise and vibration, particularly affecting residential areas near underground infrastructure. Ground-borne noise from rail traffic in tunnels can impact human health, structural integrity, and overall environmental quality. To support effective mitigation and infrastructure planning, accurate and reliable prediction models are needed.

This study developed a model and methodology for predicting ground-borne noise from railway traffic in tunnels, tailored for Swedish conditions with high-quality bedrock. Existing models are often proprietary, with limited data available for Swedish bedrock conditions, and the handling of uncertainties is often insufficiently explained. This work addresses these gaps by developing a structured, multi-stage model to support the Swedish Transport Administration projects. The methodology consists of three stages, location, planning, and construction, each adapted to the level of data available. The model is valid up to 1 kHz and incorporates a source term along with correction terms for train speed, distance attenuation, ground-to-building coupling, vibration transmission through structures, and room acoustics. Statistical uncertainty is included for each term, ensuring robust predictions.

The model is based on field measurements from the Gårda tunnel in Gothenburg and the Åsa tunnel in Varberg. To enhance understanding, numerical simulations were also conducted to investigate the effects of cracked bedrock zones and tunnel structures on vibration propagation. The simulations showed that the cracked zone causes frequency-dependent attenuation beyond the zone and amplification on the source side under idealized conditions. Tunnel structures were found to reduce vibration levels above the tunnel and introduce fluctuations at higher frequencies.

Additional field tests were conducted in a tunnel under construction using both shaker and hydraulic hammer excitations to further refine the model by assessing vibration transfer to nearby buildings. While these tests allowed for a comparison between excitation sources, no significant vibration was detected at the house level.

As a result, a methodology and detailed prediction model is proposed for ground-borne noise assessment in Swedish Transport Administration projects.

Keywords: Ground-borne noise prediction, Railway tunnel, Wave propagation in bedrock, Cracked zone.

Preface

This doctoral thesis is the result of research conducted between January 2020 and September 2025 at Chalmers University of Technology, Department of Architecture and Civil Engineering, Division of Applied Acoustics. The work was carried out in collaboration with the Swedish Transport Administration (Trafikverket), whose practical needs have strongly influenced the direction of the project. The project was also financially supported by Trafikverket. The purpose of this research has been to develop a methodology and model to predict ground-borne noise from rail traffic in tunnels in bedrock.

I am deeply grateful to my main supervisor, Patrik Höstmad, and my co-supervisor, Jens Forssén, for their continuous support and insightful guidance. Their patience, calm attitude, and consistently constructive feedback have been valuable in shaping the quality and direction of this work. Working closely with both of you throughout this journey has been deeply enriching, I have learned immensely from your knowledge, experience, and support.

Special thanks go to Wolfgang Kropp, head of the Division of Applied Acoustics, for his continuous support, empathy, and thoughtful leadership. His willingness to listen, check in, and resolve administrative issues created a strong sense of trust and reassurance during my time as a PhD student. I am truly grateful for his understanding and support throughout this journey.

I also wish to thank my colleagues at the Division of Applied Acoustics, Astrid, Jens A., Monica, Hannes, Tommi, Leon, Elin, Jannik, and Börje for their support, encouragement, and everyday kindness. Their warm presence created a positive and welcoming atmosphere.

Gratitude is also extended to the team at Trafikverket, Maria Luisa Botella, Alf Ekblad, and Magnus Källman, for their valuable input and support. Their constructive comments, as well as their provision of data, documents, and practical information, were essential to the development and application of this work.

I would also like to thank Johan Scheuer for his valuable contributions during the measurement campaigns and for sharing data, information, and practical knowledge. I am also thankful to the reference group of engineers for their constructive comments and for sharing their models and reports.

Thanks go to my close friends, especially Maryam, Amin, Asal, and Mahtab, whose support made this journey much easier. I am deeply grateful to Ehsan, who supported me throughout and helped me in many ways. From him, I have learned not only in my academic journey but also in many aspects of life. He has left a lasting impression on me.

Finally, my deepest gratitude goes out to my family, whose unconditional love has been my greatest strength throughout this journey.

List of Publications

[**Paper A**] **F. Dashti, P. Höstmad, J. Forssén**. Finite element modelling of tunnel shielding in vibration measurements of ground-borne noise. *14th International Workshop On Railway Noise (IWRN14)*, China, Shanghai (2022). *"Peer-reviewed conference paper"*.

[**Paper B**] **F. Dashti, P. Höstmad, J. Forssén**. A framework in three different project stages to predict ground-borne noise of trains in railway tunnels. *Internoise*, France, Nantes (2024).

[**Paper C**] **F. Dashti, P. Höstmad, J. Forssén**. Investigation of the relation between horizontal and vertical vibration levels on railway tunnel walls and at ground surface. *"Submitted"*.

[**Paper D**] **F. Dashti, P. Höstmad, J. Forssén**. The effect of cracked zone in bedrock on ground-borne vibration generated by underground sources. To be submitted to *15th International Workshop On Railway Noise (IWRN15)*, Spain (2025). *"Peer-reviewed conference paper"*.

[**Report**] **F. Dashti, J. Forssén, P. Höstmad**. Ground Borne Noise Model and Methodology Description. Tech. Rep. Division of Applied Acoustics, Department of Architecture and Civil Engineering, Chalmers University of Technology, Gothenburg (2025).

Contents

Part I

Overview

CHAPTER 1

Introduction

1.1 Background

Human well-being and environmental sustainability are significantly affected by noise and vibration. Noise refers to unwanted sounds that disrupt communication, cause discomfort, and lead to health problems. Vibration, on the other hand, refers to mechanical oscillations or movements, which are perceived as dynamic sensations. These phenomena can arise from various sources, including transportation systems, industrial processes, construction activities, and natural events such as earthquakes.

Railway systems, in particular, are a major contributor to noise and vibration, significantly affecting nearby communities and structures. Railway air-borne noise is typically generated by the rolling contact between train wheels and tracks, aerodynamic effects, and other mechanical sources [1]. Ground-borne vibrations, on the other hand, originate from the dynamic interaction between the train and the track, primarily at the wheel–rail contact, and propagate through the surrounding environment. Ground-borne noise is defined as the audible noise generated inside buildings as a result of ground-borne vibrations.

To mitigate the adverse effects of ground-borne noise and vibration, a systematic approach involving three key steps is required: (1) collecting relevant input data such as train characteristics, track conditions, geotechnical properties; (2) developing

methodology and predictive models to estimate noise and vibration levels; and (3) implementing mitigation measures based on the prediction to reduce the impact of noise and vibrations. This study focuses on the first and second steps: collecting relevant input data and the development of a methodology and prediction models for ground-borne noise.

Predicting ground-borne noise is essential before constructing a new railway in tunnels or on the ground surface close to residential areas and vice versa. The ground-borne noise prediction model accounts for four key factors: the source term (vibrations generation by the train-track interaction), the propagation path (how vibrations travel from the tunnel to nearby buildings' foundation and floor), the receiver term (how vibrations impact the structures above), and the sound radiation (how these structural vibrations are converted into audible noise within indoor spaces). Various models have been developed to predict ground-borne noise. Some of them are described in (section 2.7). However, more knowledge is needed to analyze ground-borne noise resulting from railway traffic in tunnels and to develop prediction models with high precision.

In general, there is a lack of published parameters specifically addressing the prediction of ground-borne noise under Swedish bedrock conditions. The characteristics of Swedish bedrock present unique challenges in this regard. It is typically of high quality with relatively few cracks, which influences how ground-borne noise propagates. The frequency range of interest for ground-borne noise in such conditions can extend up to 1000 Hz. However, findings from this study show that the upper frequency of interest is up to around 500 Hz.

To regulate ground-borne noise, the Swedish Transport Administration, Trafikverket, has established a maximum indoor noise limit of 32 dBA (time-weighting Fast) [2]. According to the current guideline, this limit may be exceeded no more than five times per average night (22:00–06:00). These standards are particularly relevant for new infrastructure projects and are specifically applied to night-time conditions to minimize disturbances during sensitive hours.

The presence of cracked zones within the bedrock further complicates ground-borne noise prediction. These discontinuities can either attenuate or amplify vibration levels depending on the location of the receiver relative to the cracked zones. Incorporating the effects of cracked zones into prediction models enhances the accuracy of ground-borne noise predictions, making it an important factor to consider in the modeling process.

The accuracy of ground-borne noise prediction is further influenced by several sources of statistical variation and uncertainties in the models. A number of factors contribute to these uncertainties, including variations in source characteristics, ground properties, wave propagation, building characteristics, and other environmental factors. To address these common uncertainties, a statistical approach is

needed to handle the data and provide more robust predictions. Empirical models have been created to predict ground-borne noise, but few studies focus on incorporating statistical methods to address the uncertainties within these predictions [3]. In this study, statistical techniques are applied to manage uncertainties in each component and to estimate the overall uncertainty of the sound pressure level within the room.

1.2 Objectives

The aim of this project is to develop a comprehensive methodology and predictive model for ground-borne noise generated by trains traveling through tunnels, especially for the Swedish Transport Administration projects. The methodology is intended to support decision-making at different stages of project development, from early planning to construction. The model should be practical to apply, flexible to update, and capable of including the most important terms influencing the ground-borne noise level.

To fulfill this aim, the project is guided by the following specific objectives:

- To identify and evaluate suitable model structures for predicting ground-borne noise from trains in tunnels.
- To determine comprehensive source terms for typical passenger and freight trains on the Swedish railway network.
- To establish a methodology and model to account for the transfer path from the source to the receiver and to determine which phenomena are important to include in the model.
- To investigate how cracked zones in the bedrock influence vibration transmission, and to assess how such features can be included in the model.
- To develop a framework for incorporating uncertainty in the model, including statistical treatment of variations in the source term, propagation path, and receiver parameters.
- To design a stepwise methodology applicable to different stages of a railway project (location, planning, and construction), with a consistent model structure and stage-specific input requirements.
- To evaluate the applicability and limitations of using in-situ measurements during the construction stage, such as those from shakers or hydraulic hammers, to refine the prediction model.

1.3 Limitation

The model is specifically designed for tunnels in dense bedrock and may not perform as accurately in other geotechnical conditions, such as loose soil. Although the model is designed to account for frequencies up to 1000 Hz, its practical applications typically focus on frequencies around 500 Hz. As a result, it may not fully capture the effects of higher-frequency vibrations in all situations. However, higher frequencies (up to 1000 Hz) may become relevant in specific cases, such as when the distance between the source and receiver is short. Furthermore, the model's validation is based on measurement data from a specific set of railway tunnels in Sweden, which could limit its applicability to other regions or types of tunnels.

To validate the proposed model, additional measurements are required. Some initial measurements were conducted in a tunnel under construction using a hydraulic hammer and shaker. However, the resulting vibrations could not be sensed or heard in the houses above the tunnel. Therefore, further measurements during the construction stage could be helpful to refine the model and improve its accuracy.

1.4 Thesis structure

This thesis is structured as follows:
Chapter 2 provides the theoretical foundation for the study, covering the source term, wave propagation, and receiver.
Chapter 3 focuses on the description and analysis of measurement data, examining source terms, wave propagation, and transfer functions to assess the impact of the propagation path on vibration levels at the receiver.
Chapter 4 provides a brief overview of the numerical simulations and their analysis results.
Chapter 5 presents an example of model application that demonstrates how the developed methodology can be used in a real-world project context.
Chapter 6 provides a concise summary of the appended publications.
Chapter 7 presents the conclusions of the study and outlines future research directions.

CHAPTER 2

Theoretical Framework

2.1 Introduction

Ground-borne vibrations refer to vibrational energy that travels through the ground, often originating from sources such as railway trains. These vibrations can propagate through the soil or bedrock and eventually reach the foundation of a building. Once transmitted into the structure, they may be felt by occupants as whole-body vibrations. The typical frequency range for ground-borne vibrations is 1–80 Hz [4].

Ground-borne noise follows a similar propagation process to ground-borne vibrations. When vibrational waves reach a building, they can induce vibrations in the building's foundation, walls, floors, and other structural components. These structural vibrations generate sound waves that are perceived as audible noise. Ground-borne noise is particularly prevalent when a railway tunnel and a building are located on the same bedrock. The typical frequency range for ground-borne noise is 20–250 Hz [4]. In areas with Swedish bedrock, this range can extend up to 1000 Hz. This is primarily due to the low attenuation properties of Swedish bedrock, which has high stiffness and low damping. As a result, the low energy dissipation, also at higher frequencies, results in low distance attenuation and significant vibrations amplitudes also at longer distances.

However, the actual frequency content that reaches nearby buildings strongly

depends on the propagation path. Complex geometry, material discontinuities (e.g., cracked zones), local damping effects, and building–foundation coupling can all limit the transmission of high-frequency components. In practice, as also observed in our measurements, ground-borne noise typically extends up to around 500 Hz, while components above this frequency often fall below the background noise level.

The vibrations generated by a train and propagating from a tunnel to the surrounding area can be described in three main stages: source, wave propagation, and receiver: source, wave propagation, and receiver. These stages play a critical role in determining the characteristics and impact of the vibrations. Figure 2.1 illustrates the propagation path of vibrations from the tunnel to a building. To effectively predict and mitigate vibration-related issues, it is essential to understand the specific contributions of each stage, which are explained in detail below.

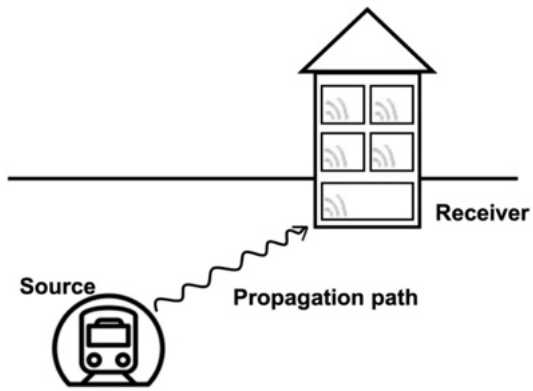

Figure 2.1: Propagation path.

2.2 Source of vibration

The primary source of vibration in railway tunnels is the movement of the train along the track and the dynamic interaction between the wheel, rail, and track structure. Various parameters influence the level of vibration generated, including train speed, axle load, car body suspension, unsprung mass, and the condition of the wheels and rails [5]–[7].

Train speed: Train speed plays a critical role in vibration levels. Higher speeds result in increased dynamic forces, leading to stronger vibrations. According to Kurzweil [8], doubling the speed of a train can cause an increase in vibration levels by 4 to 6 dB.

Axle load: Trains carrying heavy and uniform cargo, such as timber, oil, or ore, typically have higher axle loads, resulting in greater dynamic forces exerted on the track and surrounding ground. This can significantly increase vibration levels in tunnels. Doubling the axle load can increase tunnel vibration levels by 2 to 4 dB [8]. A recent study investigated the effect of axle load on ballast bed vibration and sleeper displacement, highlighting the role of Under Sleeper Pads (USPs). While USPs were found to reduce vibrations and enhance dynamic performance compared to tracks without them, the study showed that increasing axle load still resulted in significantly higher vibration acceleration in the ballast and greater dynamic displacement of the sleeper [9].

Unsprung mass: The unsprung mass, which includes components like wheels, axles, and parts of the suspension, also affects vibration levels. A reduction in unsprung mass can significantly lower ground vibrations. For example, halving the unsprung mass can reduce vibration levels by approximately 6 dB [10].

Wheel and rail condition: The condition of the wheels and rails is another key factor. Inadequate maintenance of wheels and rails can lead to significantly higher vibration levels compared to well-maintained systems with smooth running surfaces and balanced wheels. Irregularities such as wheel flats, loose rail joints, or rail corrugation can amplify vibrations up to 20 dB [11], [12].

2.3 Fundamentals of Wave Propagation

2.3.1 Wave types in ground

Within a solid medium, wave motion can be classified into body waves and surface waves. Body waves travel within the earth, whereas surface waves move along the earth's surface. Body waves consist of pressure waves (P-waves) and shear waves (S-waves). P-waves, the fastest seismic waves, move in the same direction as particle displacement. S-waves are the second fastest and move perpendicular to particle displacement. Upon reaching the ground surface, these waves transition into surface waves, with reflections also occurring. The main types of surface waves are Rayleigh waves (R-waves) and Love waves. Rayleigh waves induce a rotational movement of the surface opposite to wave direction. Love waves arise only if the top soil layer has a substantially lower wave speed than the layers below and they are relatively rare. Figure 2.2 illustrates the propagation of both wave types through the ground.

Different waves propagate at different speeds in a medium. Eq 2.1 and 2.2 show speeds of P-wave (c_p) and S-wave (c_s), respectively.

$$c_\mathrm{p} = \sqrt{\frac{E(1-\nu)}{\rho(1-2\nu)(1+\nu)}}, \tag{2.1}$$

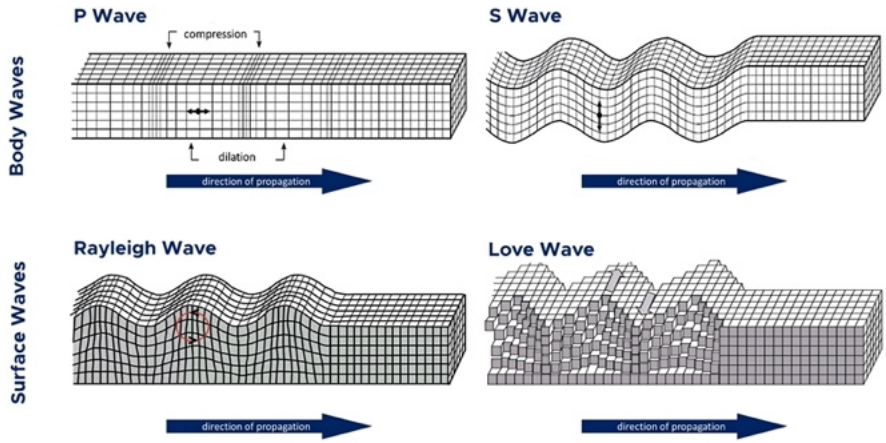

Figure 2.2: Seismic wave types. Adapted from [13].

$$c_{\mathrm{s}} = \sqrt{\frac{G}{\rho}}, \tag{2.2}$$

where E is the Young's modulus, ν is the Poisson's ratio, ρ is the density of the soil and G is the shear modulus.

R-waves can be generated by the interaction of two body waves at the ground surface. The following expression can be used to estimate the speed of the R-wave, c_{R} [14].

$$c_{\mathrm{R}} \approx \frac{0.862 + 1.14\nu}{1 + \nu} c_{\mathrm{s}}. \tag{2.3}$$

2.3.2 Wave propagation

As the distance from a vibration source increases, the vibration amplitude decreases due to two main effects: geometrical damping and material damping. Geometrical damping occurs because the wave energy spreads over a larger area as it moves away from the source. This reduction in amplitude depends on the type of source and wave but is not frequency-dependent. Material damping happens when energy is lost during each cycle of deformation as waves travel through the material. Geometrical damping affects body waves (P-waves and S-waves) more significantly than Rayleigh waves. However, Rayleigh waves still lose energy due to material damping. Because Rayleigh waves experience less attenuation, they tend to carry most of the vibration

energy at greater distances from the source.

The combined effect of geometrical and material damping can be mathematically described using Lamb's equation:

$$v = v_1 \left(\frac{r_1}{r}\right)^m e^{-\alpha(r-r_1)}, \tag{2.4}$$

where v_1 is the vibration amplitude at distance r_1 from the source, v is the vibration amplitude at distance r from the source, the exponent m is a constant that determines geometrical attenuation power based on wave type and source type, and α is the damping coefficient for the material damping. The damping coefficient measures how quickly energy is lost as vibrations travel through a material. A higher damping coefficient means faster energy dissipation. It depends on factors such as the material properties and the frequency of the vibration. Table 2.1 shows an example of the damping coefficient range for a frequency of 50 Hz.

Table 2.2 presents the exponent m for geometrical damping based on different wave types and vibration sources. When a building is far from the railway, a train can be approximated as a moving point source. Similarly, when a train passes through switches or curves, it also behaves like a point source. However, at shorter distances between the railway and a building, a train is better represented as a line source. Ground-borne noise is typically more significant at closer distances to the railway. When a train moves through a tunnel, it is generally modeled as a line source, since the train consists of sources, one at each wheel-rail contact, distributed along a line. It is often the p-waves that transfer most of the energy at longer distances, due to their higher wave speed and lower attenuation compared to shear S-waves in typical ground conditions [15]. This results in geometrical damping reducing vibration amplitude by 3 dB per distance doubling.

In some cases, vibration generation varies between bogies. This is particularly evident in freight trains, where individual wagons can be significantly heavier, and wheel flats may be present. As a result, the maximum vibration levels may be caused by specific bogies, which act more like point sources rather than contributing evenly along the train's length. Similarly, in passenger trains, factors such as wheel flats and switches can sometimes cause the train to behave more like a point load, rather than a continuous line source. These variations in bogie-induced vibrations can influence distance attenuation patterns, leading to localized amplifications or reductions in vibration levels along the propagation path.

Table 2.1: Values of damping coefficient for 50 Hz [16].

Soil class	Damping coefficient α (1/m)
Soft soils like loose clay	0.1–0.3
Firm soils like solid clay	0.03–0.1
Stiff soils like very stiff clay	0.003–0.03
Stiff bedrock	<0.003

Table 2.2: Values of the constant m [17], [18].

Wave type	Point source	Line source
P-wave	1	0.5
S-wave	1	0.5
R-wave	0.5	0

Wave equation in elastic media

The displacement field ($\mathbf{u}$) in an isotropic elastic medium is governed by the elastodynamic wave equation:

$$(\lambda + \mu)\nabla(\nabla \cdot \mathbf{u}) + \mu\nabla^2\mathbf{u} = \rho\frac{\partial^2\mathbf{u}}{\partial t^2}, \tag{2.5}$$

where λ and μ are Lamé constants, ρ is the mass density, and $\mathbf{u}$ is the displacement vector.

Assuming time-harmonic motion of the form $\mathbf{u}(\mathbf{r}, t) = \mathbf{u}(\mathbf{r})e^{-i\omega t}$, where ω is the angular frequency, the wave equation transforms to the frequency domain:

$$(\lambda + \mu)\nabla(\nabla \cdot \mathbf{u}) + \mu\nabla^2\mathbf{u} + \rho\omega^2\mathbf{u} = 0. \tag{2.6}$$

This equation serves as the basis for deriving the displacement fields due to in-plane line sources.

A Two-dimensional problems in full, homogeneous spaces subjected to unit horizontal and vertical line sources located at $x = 0$, $z = 0$ is considered here [19]. A receiver is placed at the coordinates (x, z). The response may be treated in Cartesian (x, z) or cylindrical (r, θ) coordinates.

In the frequency domain at angular frequency ω, the Green's function $g_{ij}(r, \omega)$

(with $i, j = 1, 3$, corresponding to x, z) can be written as

$$g_{ij}(r, \omega) \;=\; \frac{1}{\mu}\Big\{\, \psi\, \delta_{ij} \;+\; \chi\, \gamma_i\, \gamma_j \Big\}, \tag{2.7}$$

where μ is the shear modulus, δ_{ij} denotes the Kronecker delta, and γ_i, γ_j are the direction cosines for wave propagation. This formulation captures both shear-vertical (SV) and P-wave contributions produced by an in-plane line load. where ψ and χ are functions of the frequency ω and distance r, related to S- and P-waves, δ_{ij} is the Kronecker delta, and γ_i are the direction cosines.

Using the solutions to the Helmholtz equations, the displacement field in the frequency domain is derived. For an impulsive line source, the Green's function components in the frequency domain are expressed as:

$$\psi = \frac{i}{4}\left[H_1^{(2)}(\Omega_S) - \frac{c_s}{c_p} H_1^{(2)}(\Omega_P)\right], \tag{2.8}$$

$$\chi = \frac{i}{4}\left(\frac{c_s}{c_p}\right)^2 \left[H_2^{(2)}(\Omega_P) - H_2^{(2)}(\Omega_S)\right], \tag{2.9}$$

where $H_n^{(2)}$ are Hankel functions of the second kind, $\Omega_P = \frac{\omega r}{c_p}$ and $\Omega_S = \frac{\omega r}{c_s}$ are dimensionless frequency parameters for P- and S-waves. c_p and c_s are the P-wave and S-wave velocities in the medium.

2.3.3 Reflection and refraction

Seismic wave propagation in the ground is influenced by reflection and refraction, which occur when waves encounter boundaries between different geological layers or structures. Reflection takes place when a wave encounters a boundary and the wave is being reflected away from the boundary. The amount of energy reflected is primarily determined by the impedance contrast between the two layers, which depends on differences in density and wave speed. A greater impedance mismatch results in stronger reflection, while a smaller difference allows more energy to pass through.

Refraction, on the other hand, occurs when a wave enters a new material and changes direction of propagation due to a difference in wave speed between the two layers. This change in direction follows Snell's Law[20], where the angle of refraction depends on the relative wave speeds of the two materials. The greater the difference in wave speed, the more the wave bends upon entering the new medium.

Both reflected and refracted waves vary in amplitude and angle depending on the impedance contrast and wave speed differences between the layers. These wave interactions play a critical role in seismic wave propagation, influencing how vibrations

travel through the ground.

2.3.4 Wave coupling phenomena and challenges in underground tunnels structure

The behavior of waves inside a tunnel is complex and frequency-dependent. Low-frequency waves tend to cause the tunnel structure to oscillate as a whole, exhibiting rigid-body motion. In contrast, higher frequencies excite more complex deformation modes, including bending and shear, resulting in localized structural responses within the tunnel.

Underground railway tunnels primarily generate P-waves, which travel through the surrounding bedrock. When these waves encounter boundaries between different rock layers, part of their energy can convert into S-waves due to changes in material properties. Additionally, when seismic waves reach the ground surface, they can generate surface waves such as R-waves and Love waves, which form through the conversion of P- and S-waves at the free surface. These wave transformations, combined with variations in geological conditions, create complexities that make purely deterministic modeling challenging. Given these uncertainties, statistical models and experimental measurements provide a reliable approach to predicting wave behavior. Statistical models help account for uncertainties in the medium, offering a probabilistic understanding of wave propagation from tunnels.

2.3.5 Wave propagation in rocks

Wave propagation in rock depends on its scale and physical properties. Small rock samples are usually considered intact, meaning their wave behavior is primarily influenced by properties such as texture, density, porosity, stress conditions, and water content [21]. Large-scale rock formations, such as those in tunnel constructions, behave differently. Here, discontinuities (e.g., fractures, faults, and layer boundaries) play a major role in wave behavior. In large rock masses, wave attenuation occurs due to both material losses and impedance differences at geological boundaries. When waves encounter discontinuities, they undergo reflection, refraction, and energy loss, often generating coupling waves at these interfaces.

Wave frequency also significantly affects propagation: when the wavelength is large compared to the discontinuity (low-frequency), waves tend to transmit, while wavelengths comparable to or smaller than the discontinuity (high-frequency) result in increased reflection and scattering [22].

2.4 Effects of cracked zones on wave propagation

The presence of cracked zones in solid materials, such as bedrock, significantly affects elastic wave propagation by introducing discontinuities that lead to wave scattering, reflection, refraction, mode conversion, and attenuation. The impact of these effects depends on factors such as crack density, orientation, connectivity, and material properties [23]. To accurately model wave propagation in fractured rock, two main numerical approaches are used: Displacement Discontinuity method and Effective Medium (EM) method.

The Displacement Discontinuity method explicitly represents each fracture as a separate feature within the rock, allowing for a detailed analysis of wave interactions with individual cracks [24]. While this approach provides high accuracy, it is computationally demanding, making it less practical for large-scale problems. In contrast, the Effective Medium (EM) method models fractured rock as a homogeneous material with modified properties by incorporating the effects of cracks into the compliance matrix, potentially introducing anisotropic behavior [25]. This method is computationally efficient and widely used in engineering applications where large-scale simulations are required, such as wave propagation caused by trains in railway tunnels.

2.5 Receiver

When the vibrations propagate through the ground, they eventually reach the foundation of nearby buildings. The coupling between the ground and the foundation influences the level of vibration that is transmitted to the structure. Referring to the FTA model [26], coupling loss for the foundation in soil is measured as -5 dB for wood-frame structures, -7 dB for 1-2 story masonry buildings, -10 dB for 3-4 story masonry, -10 dB for large masonry structures on piles, and -13 dB for large masonry on spread footings. While, buildings supported directly on rock have minimal coupling loss, often considered negligible. Additionally, according to the RIVAS project [27], for the multifamily building category, vibration transmission from ground to building foundation shows minimal reduction at low frequencies (around 2 Hz) and high frequencies (around 250 Hz). However, at mid frequencies between approximately 20 and 80 Hz, a significant reduction of around 15 dB is observed, with a standard deviation of about ± 5 dB, indicating notable attenuation in this frequency range.

The vibrations travel from the foundation to various sections of the building, causing vibrations in walls, ceilings, and floors. According to [28], entire buildings may resonate at frequencies below 10 Hz, while walls and ceilings typically exhibit resonance in the range of 10–60 Hz, depending on their orientation. Floor resonances

can also lead to amplified vibration amplitudes. For example, wood-frame residential floors typically resonate between 15 and 20 Hz, and reinforced concrete slab floors between 20 and 30 Hz [29].

The perception of vibrations depends on their frequency. At certain frequencies, vibrations can be felt as whole-body sensations, known as ground-borne vibrations, or heard as low-frequency rumbling sounds, referred to as structurally radiated noise or ground-borne noise. According to Kurzweil [8], in heavy buildings, vibration levels typically decrease with height, reducing by approximately 1 to 3-4 dB per floor. In contrast, in lightweight buildings, vibration levels generally remain constant with height. However, in such buildings, vibrations on upper floors may sometimes increase due to resonances in the floor structure.

When vibrations travel through a building, they cause the walls, floors, and ceilings to vibrate, emitting noise into the surrounding spaces. The noise levels generated within a room are influenced by factors such as the size and shape of the room, the amount of sound absorption, and surfaces' vibration [30]. Based on Melke's suggestion [31], the sound pressure level in a room can be estimated by the following formula:

$$L_{\mathrm{p}} = L_{\mathrm{v}} + 10\log_{10}\sigma + 10\log_{10}\left(\frac{4S}{A}\right) \qquad \text{(dB)}, \tag{2.10}$$

where L_{p} is the sound pressure level (dB re 20 μPa), L_{v} is the vibration velocity level (dB re 50 nm/s), σ is the radiation efficiency(-), S is the vibrating surface area (m^2), and A is the absorption area of the room (m^2 Sabine). A simplified formula presented in the European project RIVAS [27] can be used for prediction at the engineering level under certain assumptions of room size 10 m^2 and the reverberation time of 0.5 s as

$$L_{\mathrm{p,av}} \approx L_{\mathrm{v,meas\text{-}floor}} + 7 \qquad \text{(dB)}, \tag{2.11}$$

where $L_{\mathrm{v,meas\text{-}floor}}$ is floor velocity level measured at mid-span (dB re 50 nm/s) and $L_{\mathrm{p,av}}$ is space average sound levels (dB re 20 μPa). Villot et al. [32] suggested a further simplified model assuming that the space-average sound level is 3 dB higher than the sound level measured in the room center as

$$L_{\mathrm{p,mes}} \approx L_{\mathrm{v,meas\text{-}floor}} + 4 \qquad \text{(dB)}, \tag{2.12}$$

where $L_{\mathrm{p,mes}}$ is the sound pressure level measured in the room center (dB re 20 μPa).

2.6 Uncertainty

Uncertainty is an inherent part of any measurement, prediction, or scientific model, reflecting the degree of confidence in the obtained results. It arises due to limitations in measurement accuracy, variability in system behavior, and simplifications in modeling approaches.

In cases where uncertainty is present, it is important to account for potential deviations from expected values. One common approach is to apply a safety factor, which introduces a conservative margin to ensure that uncertainties do not lead to unsafe or unreliable outcomes. Safety factors are widely used in engineering and design to compensate for unknowns and variations in material properties. However, safety factors are often fixed values chosen based on experience or regulations, which may result in overly conservative design, leading to unnecessary material use and increased costs.

An alternative approach is statistical analysis, particularly through standard deviation calculations. By applying the mean plus/minus two times standard deviation, a confidence interval is defined, typically covering 95% of possible outcomes in normally distributed data. This method provides a probabilistic measure of uncertainty rather than a fixed margin. Unlike safety factors, which are often experience of worst cases, standard deviation-based analysis adapts to actual data variability, making it more precise and efficient. However, this probabilistic approaches require a sufficiently large and representative dataset, and assumes that the underlying data distribution (e.g., normal distribution) is valid.

Probabilistic approaches [33] can also be used to evaluate uncertainties in computational models. However, the implementation of such methods is beyond the scope of this study.

2.7 Existing models

Various models have been developed to evaluate existing noise sources, forecast the impact of new sources, and compare noise levels across different locations.

Common approaches for predicting ground-borne noise and vibrations include empirical [8], [34], analytical [35], [36], numerical [37]–[40], and hybrid models [41]–[43]. Empirical models rely on measurement data to quickly estimate noise and vibration levels, while analytical models use physics-based mathematical formulations to provide a deeper understanding of wave propagation and vibration mechanisms. Finite Element Models (FEM) account for structural dynamics, soil-structure interactions, and complex vibrational responses, making them useful for detailed simulations. Hybrid models integrate multiple methods to improve prediction accuracy by leveraging the strengths of different approaches. The choice of model depends on factors

such as problem complexity, available data, computational requirements, and desired accuracy.

Most simplified ground-borne noise prediction models follow a structured approach, starting with a source term, followed by correction factors that account for various influencing factors such as train speed, attenuation over distance, ground-to-building coupling, and the impact of vibration levels on walls and floors in determining sound pressure levels. The correction terms are typically treated as independent, allowing for separate analysis. The following sections present some well-established models in this field.

Model suggested by Kurzweil

Kurzweil [8] proposes a method for estimating A-weighted sound pressure levels, as well as noise and vibration spectra resulting from train-induced ground-borne vibrations in buildings, presented in octave bands.

The floor vibration level, $L_{\mathrm{a(room)}}$ (dB re 10^{-6} g(rms)), in a building located near a subway, is calculated as

$$L_{\mathrm{a(room)}} = L_{\mathrm{a(tunnel\ wall)}} - C_{\mathrm{g}} - C_{\mathrm{gb}} - C_{\mathrm{b}} \qquad \text{(dB)}, \tag{2.13}$$

where $L_{\mathrm{a(tunnel\ wall)}}$ is the octave band acceleration of the wall of a subway tunnel during a train pass-by (dB re 10^{-6} g(rms)), C_{g} is the vibration attenuation due to propagation through the ground (dB), C_{gb} is the vibration attenuation (coupling loss) between the ground and the building (dB), and C_{b} is the vibration attenuation due to the propagation in the building (dB). These corrections are based on [44] and [45].

Tunnel wall vibration level, L_{a}
Measurements were taken for both ballasted and direct fixation rail fastening systems (excluding floating slab track) within concrete tunnel structures on an earth foundation.

Vibration attenuation in soil ground, C_{g}(soil)
The vibration spectrum in the soil at a specific distance from the tunnel wall is obtained by subtracting the correction presented in Figure 2.3 from the octave-band levels measured at the tunnel wall. Figure 2.3 demonstrates the reduction in ground vibration levels, C_g (soil), due to their propagation through the soil. The graph presents this reduction for several distances from the wall of a tunnel constructed in soil, across a range of frequencies.

Vibration attenuation in rock, C_{g}(rock)
In rock formations, geometric attenuation is characterized by Eq. 2.14, which is

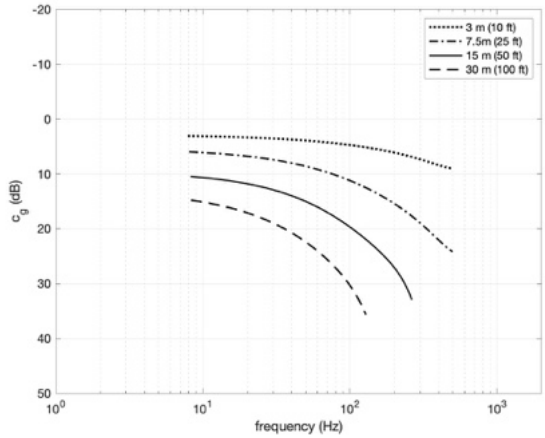

Figure 2.3: Vibration attenuation due to propagation through the ground. Adapted from reference [8].

corresponds to line source attenuation. This formula is applicable for distances reaching approximately half the length of the train.

$$C_{\mathrm{g(rock)}} = 10 \log_{10} \left(\frac{R_0 + X}{R_0} \right) \qquad \text{(dB)}, \tag{2.14}$$

where R_0 refers to the distance between a tunnel's center and its outer wall (m) and X is the distance from that surface to an observation point (m).

Coupling loss between ground and building, C_{gb}
For lightweight frame buildings and slab foundations on grade the coupling loss is 0 dB; For buildings with footings very close to the tunnel structure, a coupling loss of 10 to 20 dB can be introduced using resilient material between the building and the structure; Otherwise the coupling loss is 0 dB.

Vibration attenuation in a building, C_{b}
Vibration levels generally diminish by 3 dB per floor beginning at the ground level, though for lightweight constructions, the decrease with height is not observed.

Structure-borne noise in buildings
An estimation of the relationship between the acceleration level of the room floor, $L_{\mathrm{a(room)}}$, and the resulting sound pressure level in the room, $L_{\mathrm{p(room)}}$ (dB re 20 μPa), is provided in Eq. 2.15:

$$L_{\mathrm{p(room)}} = L_{\mathrm{a(room)}} - 20\log_{10} f + 37 \text{ (dB)}, \tag{2.15}$$

where f is the octave-band center frequency (Hz).

BanaMarkPRO model

The BanaMarkPRO model, developed by Region Stockholm (SLL), is an advancement of the Danish model "Vibration from Railway Traffic" (Banestyrelsen, 2000). It is designed to predict ground-borne vibrations in soil, providing results in 1/3-octave bands over a frequency range of 2.5 Hz to 200 Hz. Thus, the model is primarily developed for soils and not Swedish bedrock.

The model used to predict ground-borne vibration transmission from the track to the receiver is outlined below. Eqs. 2.16 and 2.17 are utilized to compute the vibration levels at the first floor and the top floor, respectively.

$$L = L_{\mathrm{Ref}} - \Delta L_{\mathrm{m}} - \Delta L_{\mathrm{e}} - \Delta L_{\mathrm{v,geo}} - \Delta L_{\mathrm{v,tab}} - \Delta L_{\mathrm{b}} - \Delta L_{\mathrm{fl}}, \tag{2.16}$$

$$L = L_{\mathrm{Ref}} - \Delta L_{\mathrm{m}} - \Delta L_{\mathrm{e}} - \Delta L_{\mathrm{v,geo}} - \Delta L_{\mathrm{v,tab}} - \Delta L_{\mathrm{b}} - \Delta L_{\mathrm{ff}}, \tag{2.17}$$

where L_{Ref} is the reference vibration level (dB re 50 nm/s), measured at $R_{\mathrm{ref}} = 8$ m from the track center, ΔL_{m} is attenuation in the ballast (dB), ΔL_{e} is vibration attenuation from the track located at embankments or cuttings (dB), $\Delta L_{\mathrm{v,geo}}$ is geometrical attenuation (dB), $\Delta L_{\mathrm{v,tab}}$ is frequency dependent hysteretic attenuation (dB), ΔL_{b} is vibration transfer from soil to foundation building (dB), ΔL_{fl} is vibration transfer from foundation to ground floor (dB), ΔL_{ff} is vibration transfer from foundation to top floor (dB).
$\Delta L_{\mathrm{v,geo}}$ and $\Delta L_{\mathrm{v,tab}}$ are calculated by Eq. 2.18 and 2.19, respectively, and other parameters are obtained from the report (Banestyrelsen 2000):

$$\Delta L_{\mathrm{v,geo}} = -11\log_{10}(R/R_{\mathrm{ref}}) \qquad \text{(dB)}, \tag{2.18}$$

$$\Delta L_{\mathrm{v,tab}} = 10\log_{10}(e^{-2\pi f\eta(R-R_{\mathrm{ref}})/c}) \qquad \text{(dB)}, \tag{2.19}$$

where $\eta = 0.03$ and the Rayleigh wave speed c is 200 m/s.

The diffuse field sound pressure level resulting from the vibrations is given by the following expression.

$$L_{\mathrm{p}} = L_{\mathrm{v(ref\ 50\ nm/s)}} + 10\log_{10}(S) + 10\log_{10}\left(\frac{4S_{\mathrm{Rad}}}{A}\right) + 3 \qquad \text{(dB)}, \tag{2.20}$$

where A is the absorption area, defined as $A = \frac{V}{6T}$ (in m^2 Sabine); V is the volume of the room (m^3), and T is the reverberation time (s). L_p is noise level in room (dB re 20 μPa), $L_{v(\text{ref } 50 \text{ nm/s})}$ is vibration level in (dB), and S_{Rad} is the area of the radiation surface (m^2).

Rivas model

The Rivas model [27] was developed as part of a European project that concluded in 2013, aiming to evaluate mitigation measures for reducing ground vibrations, ground-borne noise, and the associated annoyance caused by railway lines. The model produces 1/3-octave response spectra within a frequency range of 4–250 Hz. To estimate building vibration and the resulting ground-borne noise, four transfer functions are applied: TF1 represents the transfer function from the ground near the tracks (8 meters from the track center, as defined in RIVAS) to the free-field ground near the building; TF2 describes the transfer function from the ground near the building to the building foundations; TF3 represents the transfer function from the building foundations to the floor; TF4 corresponds to the transfer function from floor vibration to the resulting ground-borne noise inside the room.

Transfer from reference distance to ground near the building, TF1
Six transfer functions were computed to model the vibration transmission from the ground near the track (8 meters from the track center) to the ground near the building at distances of 12, 16, 20, 24, 28, and 32 meters from the track center. These calculations were performed using a 2.5D Boundary Element Method (BEM) for each specific soil type. The RIVAS project considered three different sites for analysis: homogeneous ($C_S \sim 250$ m/s), layered with increasing stiffness (from $C_S \sim 130$ m/s to $C_S \sim 350$ m/s), and soft soil ($C_S \sim 130$ m/s).

Transfer from Ground to Building Foundations, TF2
The empirical model Vibra-2 [46] was used to compute TF2, which represents the insertion loss of the building. Within the 4–250 Hz frequency range, the relative vibration response initially increased by 1 dB at 4 Hz when transferring from the foundation to the floor, then gradually decreased to approximately -11 dB between 30 and 63 Hz, before rising back to nearly 0 dB at 250 Hz. Due to limited data availability, a standard deviation of 5 dB was assumed. Additionally, the study found that softer soils or shallower foundations resulted in lower attenuation from the ground to the building foundations.

Transfer from Building Foundations to Floor, TF3
Both concrete and wood floors were considered when analyzing the vibration transfer from building foundations to the floor. The empirical model Vibra-2 was used to

determine average values for typical floor structures.

Transfer from Floor Vibration to Room Ground Borne Noise, TF4
The transfer function TF4 was applied to estimate the space-averaged sound level ($L_{\mathrm{P(av)}}$) from the vibration level at mid-span ($L_{\mathrm{v(meas)}}$). It is assumed that the floor's space-averaged velocity is lower than the mid-span velocity, while the room's space-averaged noise level is higher than the noise at the room center. This accounts for both floor and ceiling radiation, while wall contributions are neglected.

Results indicate that the relative response (TF4) was most pronounced within the 16–61 Hz frequency range, peaking at 25 dB around 30 Hz. A simplified formula for this relationship is presented below.

$$L_{\mathrm{P(av)}} \approx L_{\mathrm{v(meas)}} + 7 \qquad \text{(dB)}. \tag{2.21}$$

The reference for sound pressure level is 20 μPa, while the reference for velocity level is 50 nm/s.

HS2 model

The High Speed 2 (HS2) model[47] was developed as an extension of the HS1 model[48], a validated ground vibration prediction model used in the UK. The HS1 model was empirically derived from the analysis of over 3,000 measurements taken at train speeds of up to 300 km/h.

The HS2 model is designed to predict vibrations generated by trains traveling at speeds of up to 360 km/h, covering a frequency range of 16–250 Hz in 1/3-octave bands. In this model, it is assumed that the effective roughness of the rail and wheel is the only speed-dependent factor affecting vibration levels. Based on this assumption, the vibration spectrum ($L_{\mathrm{v2,rms}}$) at a train speed v_2 can be determined by scaling the vibration spectrum at speed v_1, as expressed in the following equation.

$$L_{\mathrm{v2,rms}}(f) = L_{\mathrm{v1,rms}}(f) + R_{\mathrm{eff}}(\lambda, \mathrm{v}_2) - R_{\mathrm{eff}}(\lambda, \mathrm{v}_1), \tag{2.22}$$

$$R_{\mathrm{eff}}(\lambda) = 10 \log_{10} \left(10^{R(\lambda)/10} + \sum_{K} 10^{L_{\mathrm{K}}(\lambda)/10} \right), \tag{2.23}$$

$$L_{\mathrm{K}}(\lambda) = R(\delta_{\mathrm{K}}) + A - \left(\frac{\log_{10} \lambda - \log_{10} \delta_{\mathrm{K}}}{B} \right)^2, \tag{2.24}$$

where, f is the frequency (center frequency of a frequency band) under consideration (Hz); $R_{\mathrm{eff}}(\lambda, \mathrm{v})$ is the effective roughness in decibels (dB), representing the displacement amplitude caused by wheel-rail interaction at the wheel-rail interface as a function of train speed v (m/s) and roughness wavelength λ (m); A and B are

constants defining the amplitude and width of the parabolic term; δ_{K} is the K^{th} sleeper or axle pitch; $L_{\mathrm{K}}(\lambda)$ is the vibration level due to the K^{th} sleeper and axle passage frequency.

The equation proposed by Bolt Beranek and Newman / Kurzweil [49] is utilized to determine the sound pressure levels (L_{pASmax}) produced by floor vibrations within the room.

2.8 Summary of model types and limitations

In most engineering prediction models for ground-borne noise, the total response is typically estimated by combining several independent factors, either through multiplication of physical quantities or, equivalently, by summing terms on a decibel (dB) scale. These terms generally represent the influence of vehicle characteristics, speed, track structure and condition, ground properties, propagation distance, vibration transmission from ground to building, structural transmission within the building, and finally, the relationship between structural vibrations and radiated sound pressure levels inside rooms. In some models, certain terms are merged into combined factors derived from empirical data.

However, many of these models do not explicitly account for the statistical variability associated with the source characteristics and wave propagation. Neglecting such uncertainties can lead to unreliable predictions and potential underestimation of vibration or noise levels, which may have safety or economic consequences. Although safety margins are occasionally applied to address this problem, incorporating statistical methods, particularly to account for variability across frequency bands and transmission paths, offers a more robust approach to managing uncertainty in ground-borne noise prediction.

Additionally, many existing models are primarily developed for soft soil conditions, where the dominant frequency range of interest is below 250 Hz. These models may not be well-suited for stiff bedrock environments, such as those found in Sweden, where higher frequency components, up to 1000 Hz, can significantly contribute to ground-borne noise.

CHAPTER 3

Field measurements for model development

3.1 Introduction

The ground-borne noise prediction model is developed using a combination of existing models, field measurements, and numerical simulations. The model aims to improve the accuracy of noise and vibration assessments by incorporating measurement data from multiple locations and refining correction terms for speed and attenuation effects.

To build and validate the model, vibration measurements were conducted in various railway tunnels and residential buildings:
Gårda tunnel: measurements were taken both inside the tunnel and in two buildings above the tunnel to analyze vibration levels and transfer functions.
Decay measurements: additional measurements were performed on the ground surface above the Gårda tunnel to examine attenuation patterns.
Floor-to-floor transmission: vibrations were recorded in a multi-story building at Övre Fogelbergsgatan 1 to evaluate how they propagate through floors.
Additional data sources: measurements from the Åsa tunnel [50] were incorporated to enhance model accuracy, and speed correction was estimated using the Håknäs tunnel method [51] .

In addition to field measurements, numerical simulations were conducted to ana-

lyze how the propagation path affects the vibration level. However, in this chapter, only the measurements and their corresponding results are presented, while the numerical simulations are described in Chapter 4.

Detailed descriptions of the measurement campaigns are provided in the following.

3.2 Measurements description

Gårda tunnel measurements

Vibration measurements were conducted in the Gårda tunnel, a 2,163-meter-long railway tunnel in Göteborg, Sweden. The tunnel runs between Gubbero in the north and Almedal in the south, following the West Coast Line. It is a double-track tunnel, excavated in bedrock, and constructed according to older Swedish railway standards. A significant number of apartment buildings and villas are situated above the tunnel. The tunnel features wooden sleepers and a ballasted track, constructed using traditional Swedish railway methods. Based on old standards [52], the ballast and sub-ballast layers in the Gårda tunnel are estimated to be approximately 0.8 m thick.

To collect data, various types of accelerometers and seismometers were mounted on the tunnel wall and sleepers. Four measurement positions were designated on both the tunnel wall and the sleepers to ensure comprehensive vibration coverage. These positions are numbered 1 to 4, arranged from north to south.

Figure 3.1 illustrates the accelerometer placement on the sleeper. Tri-axial Dytran 3143D accelerometers were mounted at four positions, measuring vibrations in three directions: vertical, horizontal parallel to the track, and horizontal normal to the track. The distances between measurement positions on the sleeper are as follows: 8.2 m between positions 1 and 2, 8.4 m between positions 2 and 3, and 14.3 m between positions 3 and 4.

Dytran accelerometers and Dytran seismometers were used to measure vibrations along the tunnel walls. Tri-axial accelerometers were placed at all measurement locations on the tunnel wall. For positions 2 and 3, seismometers were installed in both horizontal (normal to the tunnel wall) and vertical directions. These seismometers were secured using aluminum cubes, which were bolted firmly to the bedrock. In positions 1 and 4, seismometers were only mounted horizontally to capture vibrations perpendicular to the tunnel wall (see Figure 3.2).

Details of the tunnel wall measurement positions and transducer models are provided in Table 3.1. A rock hammer hitting the bedrock surface was used trying to find positions with firm bedrock. The distances between the measurement positions on the tunnel wall are as follows: 10.3 m between positions 1 and 2, 4.7 m between positions 2 and 3, and 17.7 m between positions 3 and 4.

Figure 3.1: Accelerometer position on the sleeper.

(a)

(b)

Figure 3.2: Measured locations on the tunnel wall in the Gårda tunnel: (a) positions 1 and 4 with one seismometer, (b) positions 2 and 3 with two seismometers.

To measure train speed, a speed radar was mounted on a stand near position 4, where an unobstructed view allowed for accurate data capture. The radar recorded train passages in both northbound and southbound directions, with the highest measured speed reaching approximately 110 km/h.

The measurements were conducted near the midpoint of the Gårda tunnel over three days, from March 27 to March 30, 2021. A total of 930 train passages were registered between April 27, 2021, at 04:20:00 and April 30, 2021, at 23:55:00. The recorded train types included X61, X31, X55, X14, X12, X11, X29, X52, and various

Table 3.1: Transducer positions on the tunnel wall. x denotes the vertical direction, y represents the horizontal direction parallel to the wall, and z represents the horizontal direction perpendicular to the wall.

Position	Model	Direction	Height above rail head (m)	Distance to track center (m)
position 1	Accelerometer 3293A Seismometer 3191a1	xyz z	1.75	2.75
position 2	Accelerometer 3293A seismometer 3191a1	xyz xz	1.25	2.75
position 3	Accelerometer 3293A seismometer 3191a1	xyz xz	1.35	2.75
position 4	Accelerometer 3293A seismometer 3191a1	xyz z	1.15	2.75

freight trains. However, the analysis primarily focused on X61, X31, X55, and freight trains, as other train types had a limited number of passages.

Approximately 450 of the recorded train passages occurred on the track closest to the vibration measurement locations. Table 3.2 presents the properties of the passenger trains considered, based on Figure 3.3. The weight given in the table represents the total mass of the fully equipped and functional vehicle, excluding passengers and cargo.

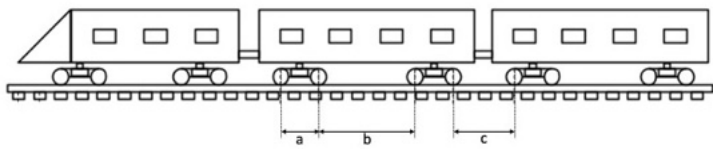

Figure 3.3: Train dimensions. Adapted from reference [4].

Table 3.2: Train characteristics [53].

Train model	Length (m)	Weight (t)	Bogie distances (m)		
			a	b	c
X55	107.2	228	2.7	16.3	4.9
X61	74.3	154	2.7	16.3	4.8
ETS (X31)	78.9	153	2.7	16.3	4.125

Buildings above the Gårda tunnel

Sound and vibration measurements were carried out in two residential buildings located above the tunnel: Prospect Hillgatan 10 and Carlbergsgatan 13 (see Figure 3.4). Prospect Hillgatan 10 is situated approximately 55 m above the tunnel floor, whereas Carlbergsgatan 13 is roughly 40 m above it. The tunnel ceiling lies about 9 m above the tunnel floor. The house measurements were conducted concurrently with those taken inside the tunnel. The measurements at each house lasted approximately 1.5 days. In the case of Prospect Hillgatan 10, transducers were installed within a 2.5 m × 2.5 m × 2.5 m bedroom where train noise was distinctly audible. This room had parquet flooring. At Carlbergsgatan 13, a ground-floor storage room measuring 1.5 m × 4 m × 2.3 m was selected for the measurements. The room had tile flooring.

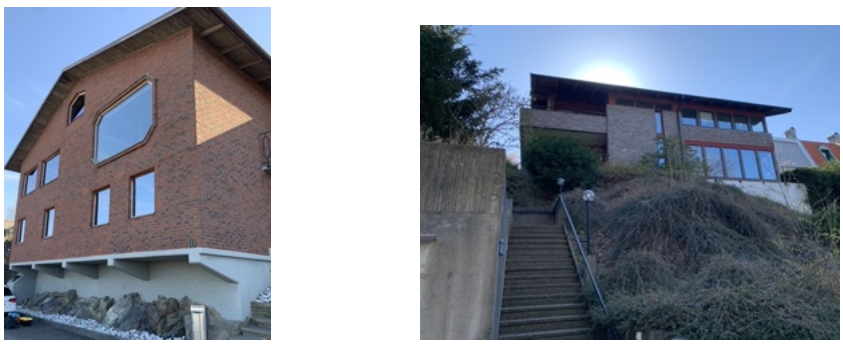

(a) (b)

Figure 3.4: Measured locations above the tunnel: (a) Prospect Hillgatan 10, (b) Carlbergsgatan 13.

The instrumentation setup in both houses included one microphone placed in the corner of the room, a seismometer (Wilcoxon model 731) positioned on the floor to record vertical vibrations, and a tri-axle accelerometer (Dytran model 3293A) mounted on the wall. Additionally, two seismometers (Wilcoxon model 731) and one tri-axle accelerometer (Dytran model 3293A) were attached to the building foundation. These seismometers captured vibrations in two directions: vertical and horizontal (perpendicular to the foundation). The sensor arrangements in the two houses are illustrated in Figures 3.5 and 3.6.

Furthermore, a speaker and two microphones were employed to determine the transfer function of sound propagation from the corner of the room to the average sound level at the room's center. One microphone was fixed in the corner, while the

other was moved around the central area of the room to measure the noise emitted by the speaker.

(a) (b)

Figure 3.5: Measured locations at Prospect Hillgatan 10: (a) inside the room, (b) on the foundation.

(a) (b)

Figure 3.6: Measured locations at Carlbergsgatan 13: (a) inside the room, (b) on the foundation.

Decay measurement

Decay measurements were performed on September 2, 2021, at the yard of Prospect Hillgatan 10, directly above the Gårda Tunnel. Receivers were positioned along a approximately 40 m line, with a spatial resolution of about 6 m, starting directly above the tunnel. Figure 3.7 illustrates the location of the receivers, with R0 positioned on the foundation.

Seismometers (Wilcoxon model 731) were placed at all positions to measure vertical vibrations perpendicular to the ground surface. Additionally, three tri-axle accelerometers (Dytran model 3293A) were installed at positions A3, A5, and A6 to provide comparative data against the seismometer recordings. The transducers (both Wilcoxon and Dytran) only captured valid signals from 10 train passages. The remaining recordings were excluded due to poor signal quality.

Figure 3.7: Location for decay measurements on the ground surface above the Gårda tunnel.

Floor-to-floor vibration measurements

To evaluate how vibration levels vary between different floors, measurements were conducted at Övre Fogelbergsgatan 1 on March 9, 2022, between 10:00 and 11:30. The building, situated above the under-construction Västlänken tunnel in Gothenburg, has ten floors and is founded directly on bedrock. Seismometers (Dytran model 3191a1) were installed in the vertical direction at four locations: the building entrance, and on floors 4, 7, and 10. A hydraulic hammer used during tunnel construction in the Västlänken served as the vibration source. It was operated once during the measurement period to ensure all sensors captured the resulting vibration signals across the floors.

(a) (b)

Figure 3.8: Example of sensor positions in Övre Fogelbergsgatan 1: (a) outside the house, (b) on floor 4.

Additional data sources

The Åsa tunnel data: according to the Åsa Tunnel report [50], vibration measurements were conducted on the tunnel wall in both vertical and horizontal directions along the Västkustbanan line between November 21, 2019, and December 23, 2019. During this period, vibrations were recorded for 2,683 train passages. The Åsa tunnel features a track with a ballast layer measuring 50 cm thick and a sub-ballast layer of 80 cm. Various train types, including freight trains and passenger trains (X61, X55, X31, X2000), passed through the tunnel during the measurement period, with the highest recorded speed reaching 196 km/h.

The Håknäs tunnel data and speed model: the Håknäs tunnel report [51] provided the basis for the speed correction model used in the locations stage of the suggested methodology. This tunnel has a recently constructed track featuring an exceptionally thick sub-ballast layer of 1.6 m and a standard ballast layer of 0.5 m. Measurements were taken at multiple locations: on the sleepers (vertical direction), on the tunnel wall (horizontal direction, perpendicular to the track), and above the tunnel. These measurements were performed using Regina trains traveling at speeds ranging from 120 to 280 km/h. Additionally, the numerical tool Findwave was employed to simulate and predict vibration levels for speeds up to 400 km/h, based on a model developed for the Citytunneln in Malmö. The vibration levels were assessed using the maximum value under time-weighting Slow conditions during train

passage.

The speed dependence model derived from the Håknäs tunnel data is presented as follows:

$$\Delta L_{\mathrm{S}} = 20 \log_{10} \frac{v}{v_{\mathrm{ref}}} \quad \text{for 80–160 km/h,} \tag{3.1}$$

$$\Delta L_{\mathrm{S}} = 10 \log_{10} \frac{v}{v_{\mathrm{ref}}} \quad \text{for 160–240 km/h,} \tag{3.2}$$

$$\Delta L_{\mathrm{S}} = 18 \log_{10} \frac{v}{v_{\mathrm{ref}}} \quad \text{for 240–320 km/h,} \tag{3.3}$$

$$\Delta L_{\mathrm{S}} = 0, \quad \text{i.e. constant, above 320 km/h,} \tag{3.4}$$

where ΔL_{S} is the speed correction term, v is the train speed of interest, and v_{ref} is the reference speed at which the source term was determined.

Measurements for construction stage

Measurements were conducted in an under-construction tunnel in Västlänken (Kvarnberget), Gothenburg to support model refinement and evaluate the impact of different excitation sources. For this purpose, a hydraulic shaker and a large hydraulic hammer were used to apply vibrations directly onto the tunnel floor (see Figure 3.9). The tests were performed during a construction phase prior to slab installation, when the tunnel floor was still covered with a layer of soft, unconsolidated concrete.

For the hydraulic hammer excitation, a steel plate was placed over a rubber mat to ensure proper energy transmission and to prevent damage to the tunnel surface. The shakers were also mounted on a steel plate, which was placed on a rubber mat. The shaker excitation was performed using a sinusoidal frequency sweep up to 1000 Hz.

Receivers were placed at several locations to monitor vibration and noise transmission: on the tunnel floor, the tunnel wall, and on the floor of a parking area in a building situated above the tunnel. Tri-axial accelerometers (Dytran) were mounted on both the tunnel floor and tunnel wall to capture vibration in three directions. Inside the building, one tri-axial accelerometer, a seismic accelerometer (Dytran 3191A1), and a microphone were installed to measure both vibrations and noise levels.

3.3 Estimated model uncertainty

The uncertainty in the predicted ground-borne noise level is estimated according to [54], by summing the variances of the individual model terms:

$$u_c^2 = \sum u_i^2. \tag{3.5}$$

(a) (b)

Figure 3.9: Source of vibration at Västlänken tunnel: (a) Hydraulic hammer, (b) Shaker.

Here, u_c represents the combined standard uncertainty, and u_i^2 is the variance of model term i. In this study, the weighting factors are assumed to be equal to 1, meaning that each model term contributes linearly and equally to the total prediction. This is justified by the model formulation, where the source term and correction terms are added or subtracted to derive the predicted levels at receiver locations. In such cases, parameter uncertainties are treated equally and remain unweighted [55]. The uncertainty in the predicted level is assumed to follow a normal distribution. To define an interval with approximately 95% confidence, it is recommended to use twice the combined standard uncertainty (i.e. $2u_c$), which corresponds to two standard deviations.

3.4 Results

This section presents a step-by-step analysis of the data collected from the measurement sites described in Section 3.2, aiming to identify the source strength and evaluate the impact of the propagation path on vibration levels.

Analysis

In general, the model is developed using time-weighting Slow instead of time-weighting Fast for several reasons. First, a substantial number of existing models and datasets

are based on time-weighting Slow. Second, it provides more stable transfer functions, whereas our analysis indicates that time-weighting Fast results in a greater statistical variation. For this reason, time-weighting Slow was chosen for predicting the ground-borne noise model. However, to facilitate comparison, sound pressure levels inside the rooms were also calculated using time-weighting Fast, with the final results presented in time-weighting Slow (Part **??**, Section 3.12).

The following analysis is conducted in 1/3-octave bands for both equivalent level and maximum level, using a simplified version of time-weighting Slow during the train passage. To determine the level, band-pass filtering is first applied at frequencies where the signal-to-noise ratio exceeds 6 dB. The data is then integrated to convert vibration acceleration into velocity, followed by the application of A-weighting using time-domain filtering. To smooth the squared velocity data, a 1-second moving average filter with constant coefficients is applied. It is acknowledged that this approach does not strictly follow the standard definition of Slow time-weighting, which requires an exponential smoothing filter with a 1-second time constant. However, a comparison between the moving average method and the standard exponential smoothing showed negligible differences for the types of signals studied here. Therefore, the moving average was used to simplify implementation, a choice that is commonly adopted in practical vibration analysis. Finally, the 1/3-octave band spectrum is computed for the 1-second interval corresponding to the maximum smoothed level.

3.4.1 Source term

During the Gårda tunnel measurements, transducers were positioned at various locations to verify the accuracy and reliability of the recorded data (see Section 3.2). For tunnels, it is generally more convenient and common to measure vibrations on the tunnel wall. Therefore, in this study, the tunnel wall is used as the reference distance for source term calculations rather than the sleeper.

Figures 3.10 and 3.11 present the vibrations captured by seismometers in the horizontal and vertical directions on the tunnel wall, shown in both the time and frequency domains. These figures demonstrate that transducers at all measured positions effectively captured the vibration signals and exhibited a consistent frequency response across the measured range. However, at Position 3, in both the horizontal and vertical directions, noticeable deviations were observed compared to the other positions, particularly at lower frequencies (below 60 Hz). Based on these observations, Positions 1, 2, and 4 were selected for further analysis in the horizontal direction, and Position 2 in the vertical direction, as they provided the most consistent data within the frequency range of interest.

Furthermore, when comparing the results from accelerometers and seismometers,

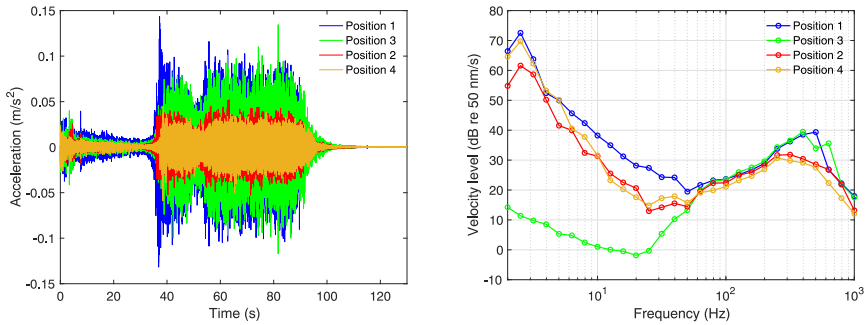

(a) (b)

Figure 3.10: Vibration related to seismometers in the time and frequency domain for the tunnel wall in the horizontal direction: (a) in the time domain, (b) in the frequency domain.

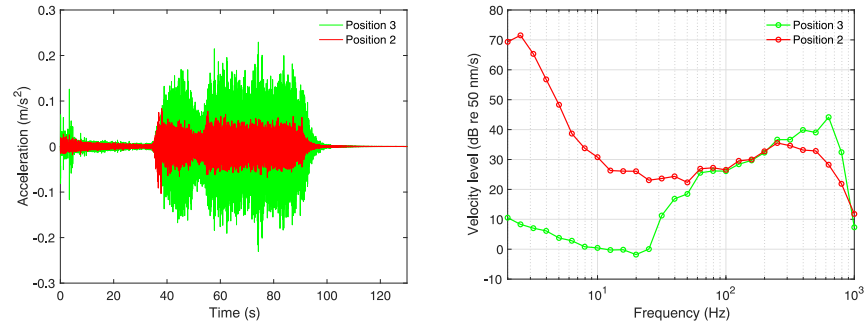

(a) (b)

Figure 3.11: Vibration related to seismometers in the time and frequency domain for the tunnel wall in the vertical direction: (a) in the time domain, (b) in the frequency domain.

it was found that the seismometers exhibited a significantly higher signal-to-noise ratio at lower frequencies (below 100 Hz). No qualified signals were captured by the accelerometers inside the houses due to low signal-to-noise ratios. Therefore, only seismometer records were used in the subsequent analysis for the development of the prediction model.

3.4.2 Train speed effect

During the measurements, the maximum train speed recorded in the Gårda tunnel was 110 km/h. To incorporate data from higher-speed trains, measurements from the Åsa tunnel, where trains reached speeds of up to 196 km/h, were included in the analysis. This decision was made due to the limited number of train passages and the absence of high-speed trains in the Gårda tunnel.

To assess the impact of train speed on vibration levels, two train categories were considered: freight trains and passenger trains. Table 3.3 presents the number of train passages and their respective speed ranges used in this study.

Table 3.3: Number of train passages.

Tunnel name	Number of trains		Train speed range (km/h)	
	Freight	Passenger	Freight	Passenger
The Gårda tunnel	18	220	18–60	43–110
The Åsa tunnel	400	1740	60–116	120–196

The influence of train speed on the maximum vibration level along the tunnel wall is analyzed to determine the speed correction term. Figure 3.12 illustrates the relationship between maximum vibration level (L_{vASmax}), versus train speed on the tunnel wall in the vertical direction. The results are based on measurements from both the Gårda and Åsa tunnels, as detailed in Table 3.3.

Figure 3.12 also includes a linear regression fit applied to the data for each train type. For each regression line, the slope (m) and the coefficient of determination (R^2) are computed and displayed in the figure. The slope m is defined by Eq. 3.6.

$$L_{\mathrm{vASmax}} = m \times 20 \log 10 \left(\frac{S}{S_{ref}} \right), \tag{3.6}$$

where S is the speed of each train, and S_{ref} is the reference speed. In this study, four reference speeds are selected for each train type in both tunnels: 160 km/h for passenger trains and 90 km/h for freight trains in the Åsa tunnel, while in the Gårda tunnel, the reference speeds are 80 km/h for passenger trains and 50 km/h for freight trains. Multiple reference speeds are used to increase accuracy, as the precision of calculations improves when the reference speed is close to the actual train speed. For small variations in train speed, the influence of speed on the final results is negligible, allowing speed adjustments to be omitted which can enhance the reliability of the results.

R^2 is defined as below:

$$R^2 = 1 - \frac{SS_{\text{res}}}{SS_{\text{tot}}}. \tag{3.7}$$

Here, SS_{res} represents the sum of squared differences between the observed values and the predicted values from the regression line, while SS_{tot} denotes the sum of squared differences between the observed values and the mean of the dependent variable. The R^2 value ranges from 0 to 1, where a value of 1 indicates a perfect match between the modeled and observed values.

Figure 3.12(b) shows a low value of R^2 value for the Åsa tunnel, indicating a poor fit of the linear regression model to the data. This suggests that the model explains only a small proportion of the variance in the dependent variable, reducing its reliability for prediction. In Figure 3.12(a), the limited number of data points for freight trains makes the calculated m value unreliable. The highest R^2 value is observed for passenger trains in the Gårda tunnel, where $m = 1.15$. This m value is close to the value of 1 found in the Håknäs speed correction model (Eq. 3.1 related to speed range 80–160 km/h).

Determining reliable m values for the Gårda and Åsa tunnels is challenging based on the obtained results. This challenge becomes more significant at higher train speeds due to the low R^2 value in the Åsa tunnel, indicating high uncertainty. Therefore, instead of deriving new correction factors, it is more appropriate to adopt the existing Håknäs speed correction model, which is developed based on Regina trains and accounts for train speeds ranging from 80 km/h to beyond 320 km/h.

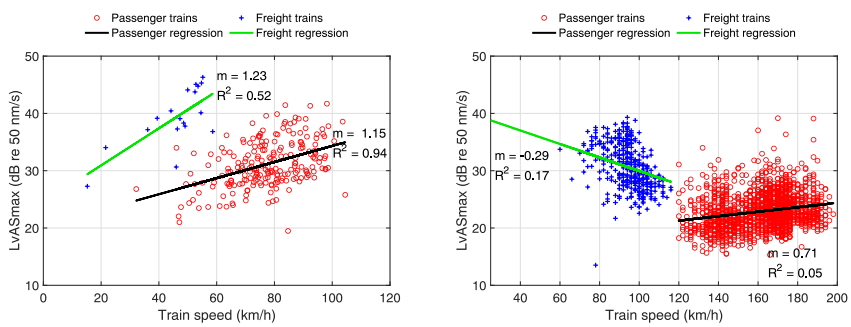

Figure 3.12: Maximum vibration level versus train speed on the tunnel wall in the vertical direction and the regression line for each train type: (a) in the Gårda tunnel, (b) in the Åsa tunnel.

The Håknäs speed correction model (Eq. 3.1 to Eq. 3.4) is applied in this study to

adjust the single vibration level value in the prediction. Additionally, the HS2 model is utilized for spectrum scaling, as described in Eq. 2.22 to 2.24. Further details on the implementation of the HS2 speed correction within the prediction model can be found in Section 3.5 of Part **??**.

The vibration level on the tunnel wall in both the Gårda and the Åsa tunnels is reproduced for passenger and freight trains using Eq. 3.1 to Eq. 3.4 to evaluate the accuracy of the Håknäs speed correction model in our predictions. The validation process is carried out in several steps. First, the maximum vibration level is determined for each train passage on the tunnel wall, and the Håknäs speed correction model is applied to estimate the source strength at the reference speed for each train type in both tunnels. Next, the arithmetic mean and standard deviation (STD) of the source strength are computed for each train category. Finally, the Håknäs speed correction model is applied to different statistical levels, including the average source strength, the average plus one STD, the average plus two STDs, and the average plus three STDs.

Figure 3.13 illustrates the relationship between the predicted and calculated L_{vASmax} and train speed for different train types in each tunnel. In the figure, lines represent the predicted model, while dots correspond to the calculated L_{vASmax} for individual train passages. The results indicate that the reproduced model, incorporating the Håknäs speed correction model plus two times the standard deviation, effectively encompasses all train passages in the Gårda tunnel. In the sa tunnel, this model (average source strength + 2STD) accurately represents all freight train passages and captures approximately 95% of the passenger train passages.

3.4.3 The effect of track type

The prediction model incorporates measurements from the Åsa tunnel to estimate the source term for new ballasted tracks, while measurements from the Gårda tunnel are used to define the source term for older ballasted tracks (see Part **??**, Section 3.4). In the model, untreated ballasted track conditions are used as the reference case. To assess the influence of track condition on vibration levels, the source strength at maximum vibration level is analyzed for each train type in both tunnels.

This analysis involves calculating the source strength for each passage based on the maximum vibration level, corrected for train speed using the HS2 speed correction model in the vertical direction on the tunnel wall. As described in Section "Train speed effect", the HS2 model is used for spectral speed correction. The arithmetic average of source strength is then computed over multiple passages for each train type.

Figure 3.14 compares the averaged results between the two tunnels. The red dash-dotted lines represent source terms from the Gårda tunnel adjusted to the reference

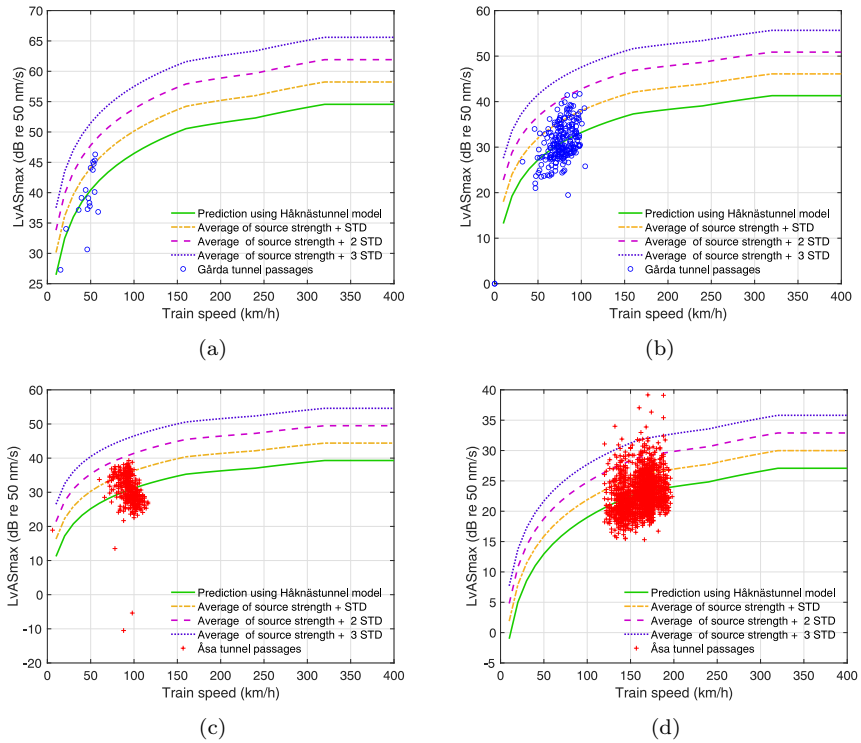

Figure 3.13: Reproduced vibration level on the tunnel wall using the Håknäs speed correction model in average, average plus one standard deviation (STD), average plus two STD, and average plus three STD: (a) freight train in the Gårda tunnel, (b) passenger train in the Gårda tunnel, (c) freight train in the Åsa tunnel, (d) passenger train in the Åsa tunnel.

speeds of the Åsa tunnel. The green solid lines show the Gårda tunnel source terms at their own reference speeds (80km/h for passenger trains and 50km/h for freight trains), and the blue dashed lines represent the Åsa tunnel source terms at its own reference speeds (160km/h for passenger trains and 90km/h for freight trains).

The number of train passages and corresponding speed ranges used in this comparison are listed in Tables 3.4 and 3.5.

According to Figure 3.14, the vibration levels observed in the Gårda tunnel are generally higher than those recorded in the Åsa tunnel across all train types. This

difference can be attributed to the Gårda tunnel being an older track, with a different type of sleeper (wooden) to the newer Åsa tunnel. Anomalies in the Åsa tunnel results are also noted, particularly a sharp increase in vibration levels above 630 Hz. This unexpected rise may be due to transducer mounting issues during the measurements.

Despite these differences, both tunnels show similar spectral trends between 40 and 400 Hz for passenger trains, and between 30 and 630 Hz for freight trains. Mismatches at lower and higher frequencies may result from variations in ballast thickness, sleeper types, and the higher train speeds in the Åsa tunnel than the Gårda tunnel.

Additionally, to investigate the effect of reference speed selection, the source term for the Gårda tunnel is plotted using two different reference speeds: its own (80 km/h for passenger and 50 km/h for freight) and the reference speed used in the Åsa tunnel (160 km/h for passenger and 90 km/h for freight). As shown in Figure 3.14, the source term scaled to its own reference speed (green line) exhibits a smoother frequency spectrum, while the scaling to Åsa's reference speed (red dashed line) introduces irregularities at some frequencies. This highlights that choosing a reference speed close to the actual train speed improves the stability and realism of the derived source term.

Table 3.4: Number of train passages in the Gårda tunnel and in the Åsa tunnel.

Tunnel name	Number of trains			
	Freight	X55	X61	ETS (X31)
The Gårda tunnel	18	10	155	66
The Åsa tunnel	400	330	140	1300

Table 3.5: Speed ranges related to train passages mentioned in Table 3.4.

Tunnel name	Speed range (Km/h)			
	Freight	X55	X61	ETS (X31)
The Gårda tunnel	18–60	60–94	47–110	32–103
The Åsa tunnel	60–116	122–196	120–184	120–196

3.4.4 Train types effect on vibration levels

This section examines the influence of three types of passenger trains, X61, X55, and ETS (X31), as well as freight trains, on the maximum vibration level along the

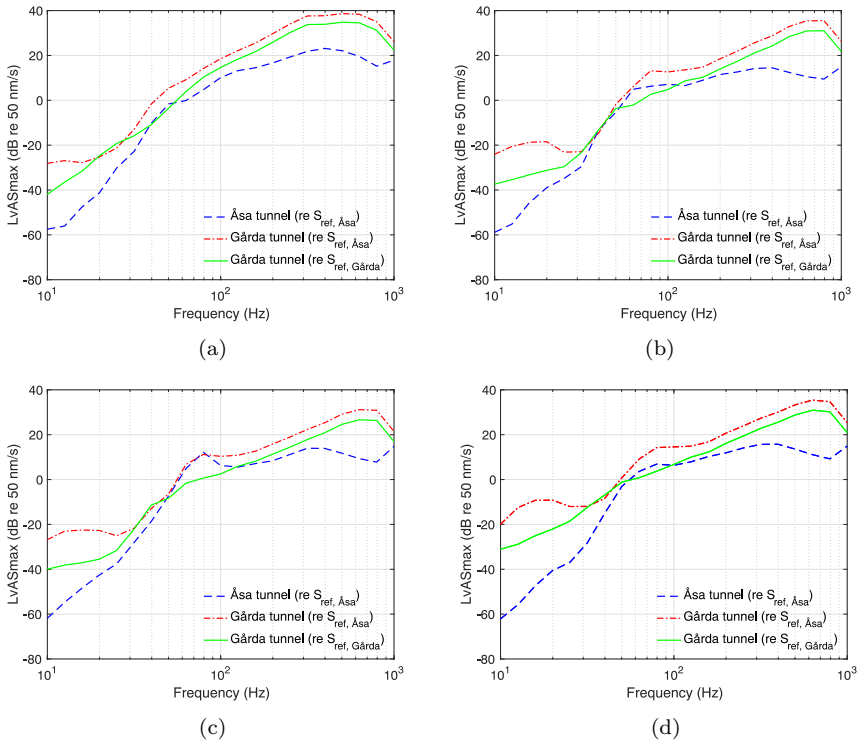

Figure 3.14: The effect of track type on the maximum level of source strength for each train type: (a) Freight train, (b) X55, (c) X61, (d) ETS (X31).

tunnel wall. The number of train passages analyzed for each train type is provided in Table 3.4. For each passage, the maximum source strength on the tunnel wall is calculated using the same methodology described in the previous section, "The effect of track type".

Figure 3.15 presents the maximum vibration levels as a function of frequency along the tunnel wall in the vertical direction for each tunnel. The results show that, in both tunnels, freight trains generally produce higher vibration levels than passenger trains at frequencies above approximately 70 Hz. Additionally, for passenger trains, the three types (X61, X55, and ETS) exhibit similar vibration levels above 50 Hz in the Gårda tunnel and above 10 Hz in the Åsa tunnel.

As discussed in the previous section, "The effect of track type", the results from

the Åsa tunnel exhibit an unexpected increase in vibration levels above 630 Hz. To mitigate this issue, an extrapolation was performed for frequencies exceeding 630 Hz. The slope derived from the Gårda tunnel data in the same frequency range (see Figure 3.15(a)) was applied to extend the Åsa tunnel spectrum. This approach ensures a smoother and more physically reasonable curve, enabling the calculation of a representative single maximum level value and the construction of the source spectrum in 1/3-octave bands.

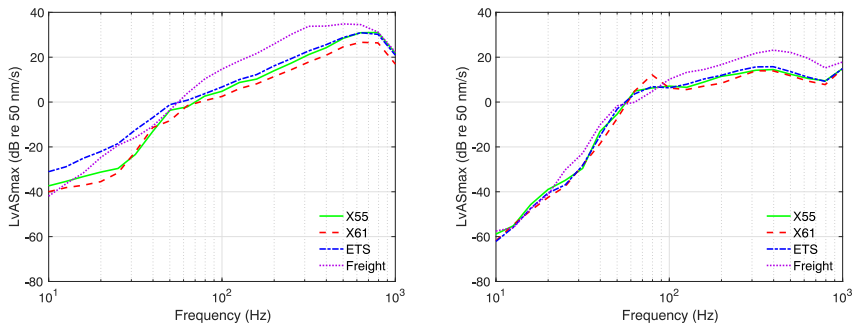

Figure 3.15: The effect of train type on maximum vibration level in the vertical direction at different frequency ranges: (a) in the Gårda tunnel, (b) in the Åsa tunnel.

Table 3.6 presents the single-value maximum vibration levels for various train types in both the Åsa and Gårda tunnels. As shown in the table, the results for the three different passenger train types are closely aligned within each tunnel.
Consequently, based on the findings in Figure 3.15 and Table 3.6, the three passenger train types (X61, X55, and ETS) exhibit sufficiently similar behavior to be grouped into a single category, while freight trains can be considered as a separate category.

Table 3.6: The average maximum value of vibration on the tunnel wall in the vertical direction in time-weighting Slow for various train types.

Train types	L_{vASmax} Gårda tunnel (dB)	L_{vASmax} Åsa tunnel (dB)
X55	34	23
ETS	34	24
X61	31	22
Freight	40	31

3.4.5 Vibration distribution across bogies

This section investigates how vibrations are distributed across train bogies during each passage to evaluate how vibrations attenuate with increasing distance from the track. The aim is to assess whether the train behaves more like a line source or a point source, thereby improving understanding of ground-borne vibration propagation.

The analysis uses vibration data from 206 passenger trains (including X61 and ETS models) and 18 freight trains, recorded in the Gårda tunnel. The first step involves identifying the vibration contribution from individual bogies. This is achieved by applying the Time Weighting Fast (L_{pF}) method to each train passage as a function of time, which enables the detection of vibration peaks associated with individual bogies. The maximum vibration level from each bogie is then extracted, providing a detailed view of how vibrations are distributed along the train in each passage.

Once the bogie-specific vibration levels are obtained, their spatial distribution is analyzed to determine whether vibrations are evenly distributed along the train or if certain bogies generate disproportionately high levels. To visualize this, two sets of statistical plots are generated and presented in Figures 3.16 and 3.17.

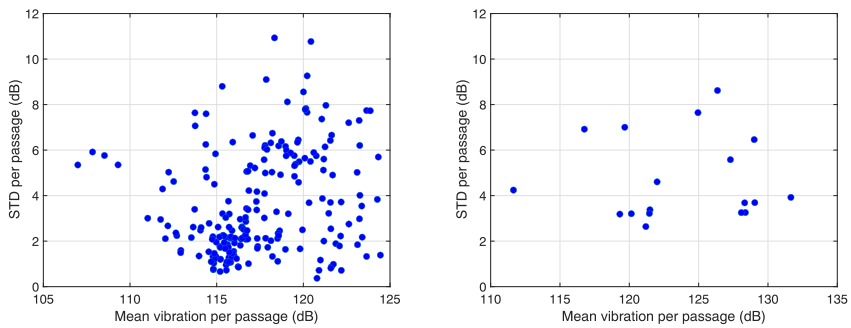

(a) (b)

Figure 3.16: Standard deviation (STD) of vibration levels across bogies for each passage: (a) passenger train, (b) freight train.

Figure 3.16 displays the standard deviation (STD) of bogie vibration levels plotted against the mean vibration level for each passage. Both the mean and standard deviation are calculated as arithmetic values. The aim is to evaluate the spread of vibration contributions across bogies in both passenger and freight trains. The figure shows no clear relationship between mean vibration level and standard deviation for

either train type. In both passenger and freight trains, STDs vary across a broad range. However, when focusing on the proportion of passages with higher variability, it is found that approximately 17% of passenger train passages and 27% of freight train passages have STDs exceeding 6 dB. This indicates that while high variability occurs in both train types, freight trains exhibit a slightly higher tendency toward uneven bogie-induced vibration levels.

Figure 3.17 presents histograms of the difference between the maximum bogie vibration and the mean for each train passage. For passenger trains (Figure 3.17(a)), the majority of passages fall within the range of 2 to 6 dB, with a gradually decreasing number of passages as the difference increases. A small number of passages exceed 10 dB, indicating occasional instances where one bogie generates noticeably higher vibrations than the others.

In contrast, freight trains (Figure 3.17(b)) exhibit a distribution that is more dispersed across the 6–16 dB range. Although the number of passages is limited, several cases show a difference greater than 10 dB, suggesting that in some freight train passages, a single bogie may dominate the overall vibration profile. This could potentially be related to uneven loading or mechanical conditions, such as wheel flats.

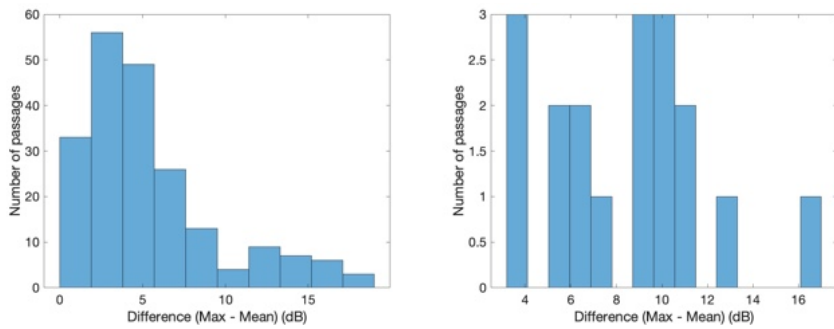

(a) (b)

Figure 3.17: Distribution of difference between the maximum bogie vibration and the mean vibration for each passage: (a) passenger train, (b) freight train.

Evaluating line vs. point source behavior based on bogie vibration distributions

To systematically analyze vibration attenuation from the track, the distribution of vibrations along the train, particularly between bogies, is used to examine how vibration decays with distance from the train. The aim is to evaluate whether the overall source behavior resembles that of a line source or a point source, based on realistic bogie excitation patterns.

Receivers are positioned perpendicular to the train at the bogie with the highest vibration level, covering distances from the track centerline at 0.5 m intervals up to 1000 m. The reference distance is set at 4.2 m. The distances between bogies are selected according to realistic spacing values ([16.3, 4.8] m), as listed in Table 3.2. For each train passage, the geometrical attenuation is calculated, and statistical analysis is applied across all 206 passenger train and 18 freight train passages. The arithmetic mean and standard deviation (STD) of vibration levels are computed at each distance and compared against reference slopes of 3 dB (line source) and 6 dB (point source) per doubling of distance. The resulting attenuation plots in logarithmic scale (see Figure 3.18) illustrate how vibration levels decrease with distance based on bogie alignment and source strength distribution.

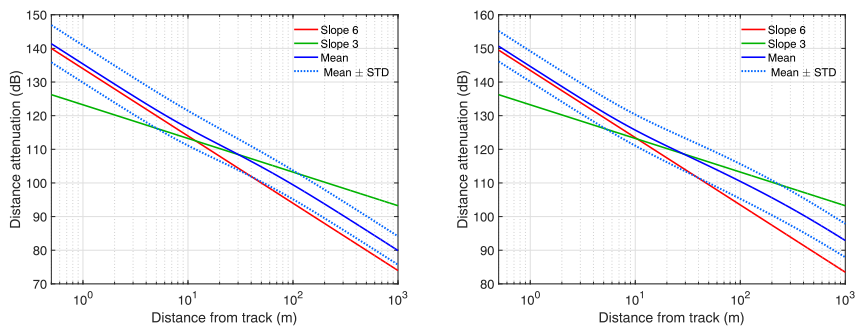

Figure 3.18: Attenuation of vibration levels with distance compared to 3 dB and 6 dB reference slopes: (a) passenger train, (b) freight train.

According to the figure, for both passenger and freight trains, the attenuation curves generally follow a slope close to 6 dB per distance doubling specially at short distances below 10 m and beyond 100 m. However, in the key range of 10–100 m, the attenuation rate tends to be less than 6 dB, often approaching around 5 dB.

For freight trains, this trend is expected, as individual bogies can dominate the

vibration signal due to uneven wagon loading or mechanical issues, such as wheel flats. While passenger trains typically produce more uniform excitation, localized effects like wheel flats or track irregularities can also lead to behavior closer to a point source.

A theoretical worst-case scenario assumes that all bogies generate equal and strong excitation, such as in the case of widespread wheel flats. In such a case, the attenuation would approach 3 dB per distance doubling. However, this situation is rarely encountered in practice. It can be concluded that assuming 6 dB per doubling is generally too strong for most real-world applications. In contrast, a 3 dB attenuation rate serves as a conservative and robust estimate, especially in design-sensitive or safety-critical contexts, where underestimating vibration levels must be avoided. If more train passages are evaluated, one might justify using a less conservative distance attenuation based on statistical evidence.

3.4.6 Propagation from tunnel wall to house

To evaluate how vibration levels vary between two locations, a transfer function is computed as a function of frequency. In this context, the transfer function represents the change in vibration level between two points during a train passage. This study estimates transfer functions from the tunnel wall to two residential locations, Carlbergsgatan 13 and Prospekt Hillgatan 10, by analyzing both vertical and horizontal vibration components. The evaluation includes both maximum and equivalent vibration levels caused by freight and passenger trains.

Before conducting the analysis, the signal-to-noise ratio (SNR) was assessed to define the valid frequency ranges for reliable transfer function estimation. A frequency band is considered valid if the SNR exceeds 6 dB. On the tunnel wall, in both measured directions, the signal consistently dominates over noise within the frequency range of 1–1000 Hz, for both train types. However, the valid frequency ranges within the buildings vary depending on location and train type. These valid frequency intervals, applicable to both vibration directions, are summarized in Table 3.7.

Figure 3.19 presents an example of measurement results for the signal-to-noise ratio (SNR) and transfer function between the tunnel wall and Prospect Hillgatan 10 in the vertical direction. In Figure 3.19(a), the SNR is shown for both the tunnel wall and the building foundation for a representative freight train passage. The results indicate that on the tunnel wall, signal levels remain consistently above noise levels across the full frequency range. In contrast, for the building foundation, the SNR exceeds 6 dB only within the range of 60–600 Hz, which is therefore used as the valid interval for estimating the transfer function for freight trains.

Figure 3.19(b) displays the corresponding transfer function in the vertical direction

Table 3.7: Valid frequency range inside houses for both vertical and horizontal directions.

House	Position	Valid frequency range (Hz)	
		Freight train	Passenger train
Carlbergsgatan 13	Foundation	60–400	60–250
	Floor	60–500	60–400
Prospekt Hillgatan 10	Foundation	60–600	60–500
	Floor	60–400	60–250

across this valid frequency range. The attenuation begins around –12 dB at 63 Hz and increases to –33 dB at 500 Hz, suggesting that higher frequencies are more strongly attenuated than lower ones. A similar pattern is observed for passenger trains in Figures 3.19(c) and (d), although the valid frequency range for passenger data is slightly narrower, spanning 60–500 Hz.

The calculated transfer function from the tunnel wall to the building's foundation and floor at Carlbergsgatan 13 and Prospekt Hillgatan 10 are shown in Figures 3.20 and 3.21, respectively. The transfer function for both equivalent and maximum levels is presented here.

Figure 3.20 illustrates the vibration transmission from the tunnel wall to the building at Carlbergsgatan 13, showing both maximum and equivalent levels based on measurements from six freight train and 120 passenger train passages. The transfer functions are derived from three valid sensor positions in the horizontal direction and one in the vertical direction on the tunnel wall, to the foundation and floor of the building. The final transfer function is calculated using an arithmetic average of these results.

As shown in Figures 3.20(a) and (b), vertical direction measurements exhibit greater attenuation in vibration transmission from the tunnel wall to the building foundation compared to the horizontal direction. The results also indicate that low-frequency vibrations experience less attenuation, while higher frequencies are more strongly damped. Additionally, the transfer functions for maximum vibration levels appear consistent across both freight and passenger trains, whereas more noticeable differences are observed in the equivalent levels. Figures 3.20(a) and (b) reveal a consistent peak near 200 Hz in the vertical direction at the foundation of Carlbergsgatan 13. This peak is observed across all train passages, regardless of timing, and is also present in the background noise measurements. The recurring nature of this feature suggests that it may be caused by resonance linked to a background source.

Figures 3.20(c) and (d) display the transfer function between the tunnel wall and

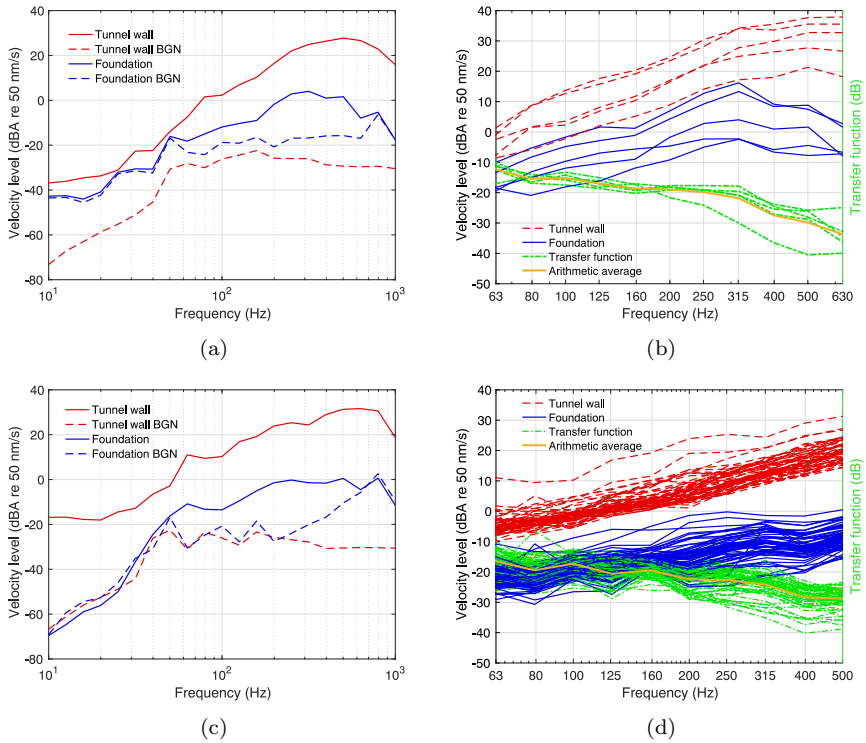

Figure 3.19: Transfer function from tunnel wall to the foundation in vertical direction at Prospect Hillgatan 10: (a) equivalent vibration levels for a single freight train with background noise (BGN), (b) transfer function for all freight train passages, (c) equivalent vibration levels for a single passenger train with background noise (BGN), (d) transfer function for all passenger trains.

the floor level of the building. The overall trend is similar to that seen in Figures 3.20(a) and (b), which represent the transmission to the foundation. However, the attenuation from the tunnel wall to the floor is generally greater, particularly when considering the maximum vibration levels.

Figure 3.21 presents the transfer functions for both maximum and equivalent vibration levels from the tunnel wall to the building at Prospect Hillgatan 10, based on data from five freight and 100 passenger train passages. As shown in Figures 3.21(a) and (b), the attenuation of vibration between the tunnel wall and the foundation is

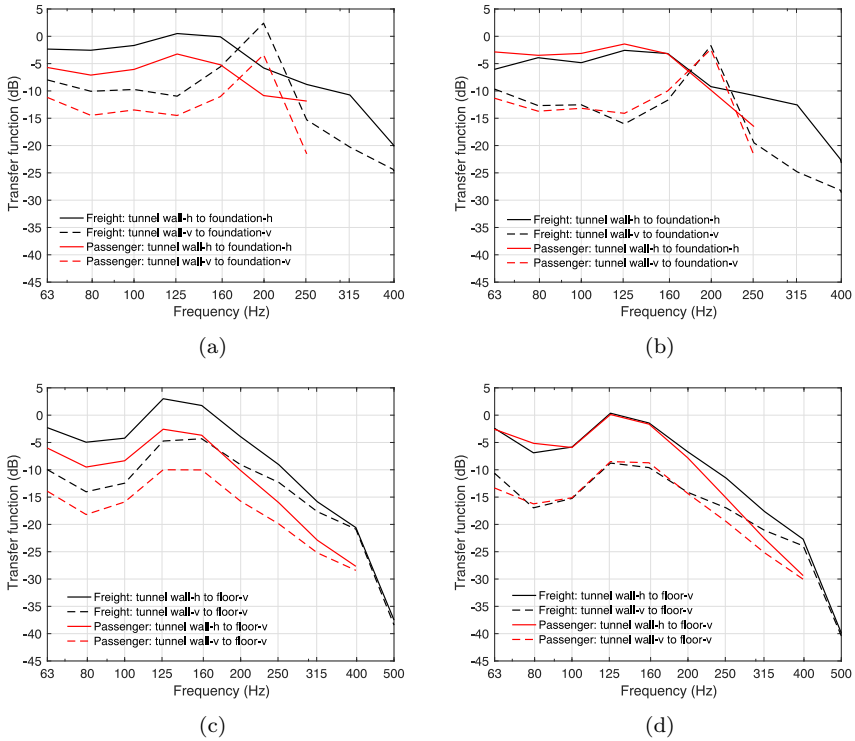

Figure 3.20: Arithmetic average of the transfer function from the tunnel wall in horizontal (-h) and vertical (-v) directions to the foundation and floor of Carlbergsgatan 13 for passenger and freight trains: (a) tunnel wall to the foundation for equivalent level, (b) tunnel wall to the foundation for maximum level, (c) tunnel wall to the house floor for equivalent level, (d) tunnel wall to the house floor for maximum level.

consistent with the trends observed at Carlbergsgatan 13.

In Figures 3.21(c) and (d), the transfer function from the tunnel wall to the floor is analyzed. In the vertical direction, the attenuation between the tunnel wall and the floor is observed to be less than that between the wall and the foundation. Additionally, an apparent amplification is noted when comparing the horizontal component on the tunnel wall to the vertical response on the floor. This is attributed to the lower vibration levels in the horizontal direction at the tunnel wall compared to the vertical component. These findings suggest that the vertical direction is more

representative of the actual vibration amplitude or energy and is therefore more suitable for use in the source characterization.

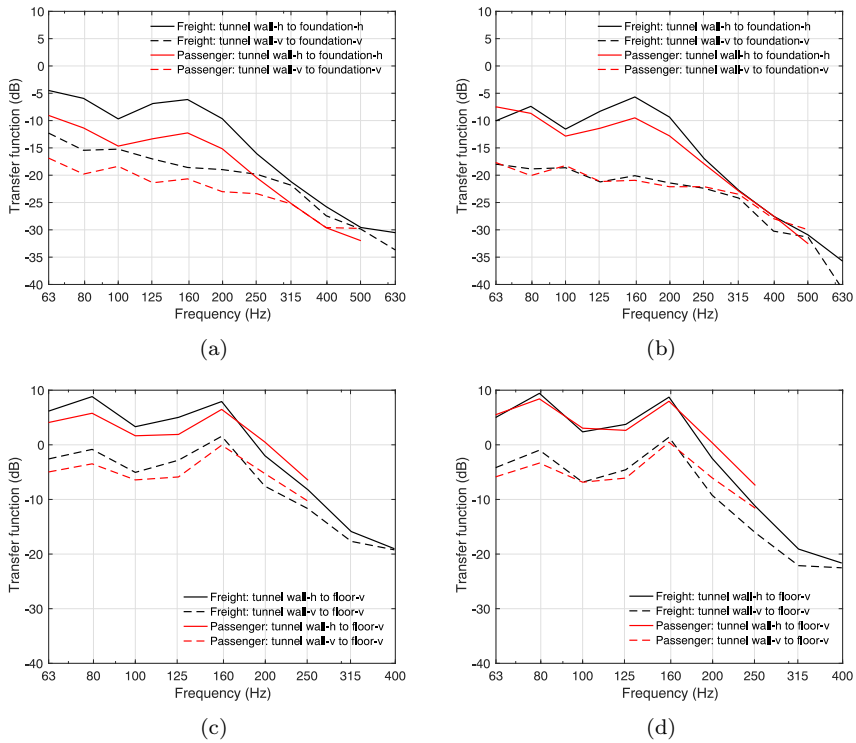

Figure 3.21: Arithmetic average of the transfer function from the tunnel wall in the horizontal (-h) and vertical (-v) directions to the foundation and floor of prospect Hillgatan 10 for passenger and freight trains: (a) tunnel wall to the foundation for equivalent level, (b) tunnel wall to the foundation for maximum level, (c) tunnel wall to the house floor for equivalent level, (d) tunnel wall to the house floor for maximum level.

3.4.7 Coupling loss at foundation

To evaluate the coupling loss factor, transfer functions between the foundation and floor were calculated for five freight train passages at Prospekt Hillgatan 10 (Figure 3.23) and six at Carlbergsgatan 13 (Figure 3.22), both of which are buildings

constructed directly on bedrock. The analysis focuses on the frequency range of 60–400 Hz, where the signal-to-noise ratio is sufficiently high in both the vertical and horizontal directions (see Table 3.7).

At Carlbergsgatan 13, as shown in Figure 3.22, the coupling loss remains close to 0 dB for both directions. A peak observed near 200 Hz in the vertical direction is attributed to background noise and can therefore be disregarded. In contrast, at Prospekt Hillgatan 10, the transfer function indicates an apparent amplification of approximately 10 dB between the foundation and the floor (Figure 3.23). This is likely due to resonances introduced by the parquet flooring, which can amplify vibrations at certain frequencies.

Given this, the results from Prospekt Hillgatan 10 are considered less reliable for estimating coupling loss, and only the measurements from Carlbergsgatan 13 are used in the final model.

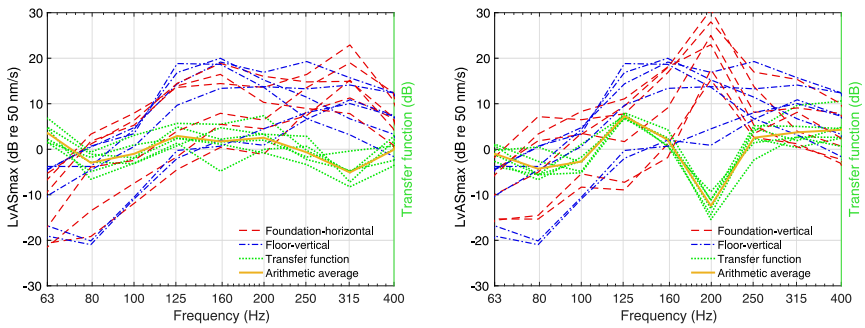

(a) (b)

Figure 3.22: Vibration level and transfer function from foundation to floor at Carlbergsgatan 13 in vertical and horizontal directions: (a) horizontal direction, (b) vertical direction.

3.4.8 Floor-to-floor correction

Valid measurements taken at Övre Fogelbergsgatan 1 were used to assess how vibration levels vary across different building floors, as illustrated in Figure 3.24. Transfer functions between floors were calculated across a range of frequencies, and the mean values shown in the figure represent the arithmetic average attenuation per floor.

According to the results for the maximum vibration level, the attenuation between floors 1 and 4 is approximately 0.75 dB per floor, while between floors 4 and 7, the attenuation increases to around 3.5 dB per floor, averaged over the valid frequency

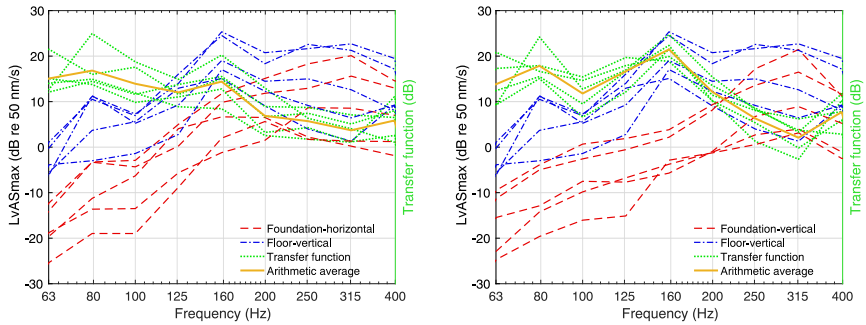

(a) (b)

Figure 3.23: Vibration level and transfer function from foundation to floor at Prospect Hillgatan 10 in vertical and horizontal directions: (a) horizontal direction, (b) vertical direction.

range. This indicates that higher floors experience greater attenuation than lower ones.

When a single value is used to represent attenuation across all floors, the result is approximately –2 dB per floor, which aligns well with estimates from other models such as those in [26] and [8]. Additionally, the observed frequency-dependent behavior indicates that vibrations below 300 Hz are more strongly attenuated on the lower floors, while vibrations above 300 Hz are more attenuated on the higher floors.

3.4.9 Vibration to noise correction

Data obtained from Prospect Hillgatan 10 and Carlbergsgatan 13 were analyzed to investigate the relationship between floor vibrations and resulting ground-borne noise within rooms. Figures 3.25 and 3.26 present the transfer functions from floor vibration to sound pressure levels measured at the room corner in each building.

As shown in Figures 3.25(a) and 3.26(a), the valid frequency range, defined by a signal-to-noise ratio exceeding 6 dB, spans approximately 60–400 Hz. Figures 3.25(b) and 3.26(b) display the maximum floor vibration level, the corresponding sound pressure level, and the resulting transfer function as a function of frequency for five freight train passages at Prospect Hillgatan 10 and six at Carlbergsgatan 13. From the results, the average transfer function between floor vibration and sound pressure level in the room corner is approximately 25 dB.
In the conducted measurements, microphones were positioned in the corners of the rooms, where sound pressure levels are typically elevated due to boundary reflections.

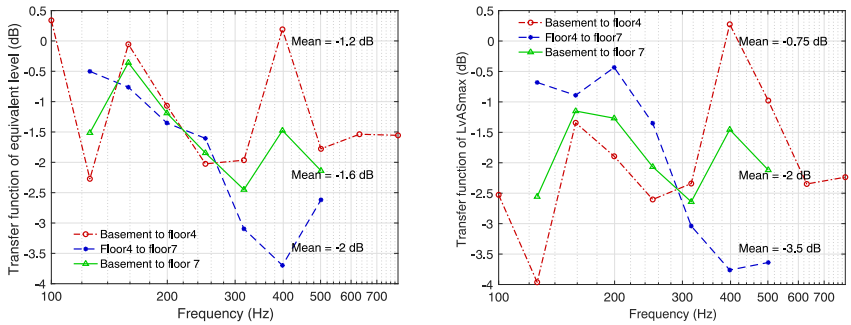

(a) (b)

Figure 3.24: Floor attenuation versus frequency and mean value of attenuation per each floor (Mean) in Övre Fogelbergsgatan 1: (a) equivalent level, (b) maximum level (time-weighting Slow).

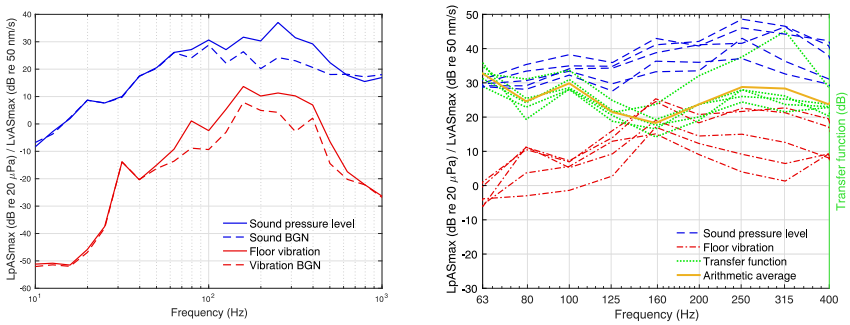

(a) (b)

Figure 3.25: Vibration level and transfer function from floor vibration to room ground-borne noise at prospect Hillgatan 10: (a) vibration and sound level, including background noise (BGN) for a single freight train, (b) transfer function for six freight trains.

However, for ground-borne noise assessments, the average sound pressure level within the room's interior is the relevant indicator. Figure 3.27 illustrates the transfer function between the sound pressure level measured in the corner and that in the center of the room, presented in 1/3-octave bands.

The results show that at Prospect Hillgatan 10, the transfer function ranges be-

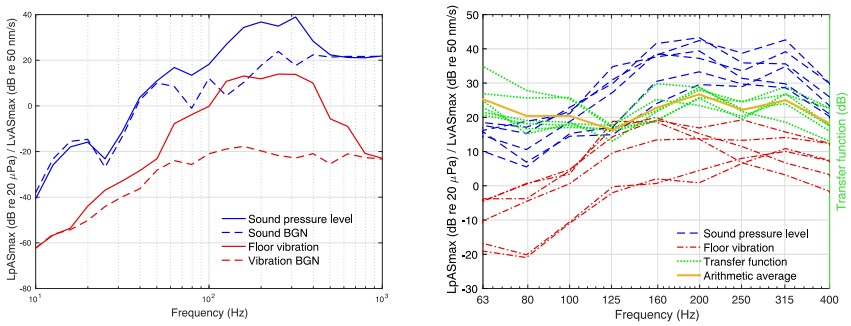

(a) (b)

Figure 3.26: Vibration level and transfer function from floor vibration to room ground-borne noise at Carlbergsgatan 13: (a) vibration and sound level, including background noise (BGN) for a single freight train, (b) transfer function for six freight trains.

tween 1 and 10 dB, depending on the frequency. At Carlbergsgatan 13, the variation is broader, ranging from approximately –10 to 10 dB across the frequency spectrum.

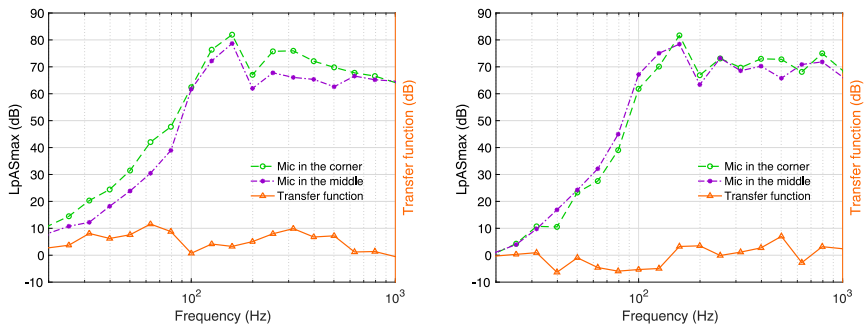

(a) (b)

Figure 3.27: Transfer function from the microphone in the corner to the microphone in the middle: (a) Prospect Hillgatan 10, (b) Carlbergsgatan 13.

Figure 3.28 shows the transfer function from floor vibration to sound pressure level in the middle of the room using the transfer function calculated from Figure 3.27.

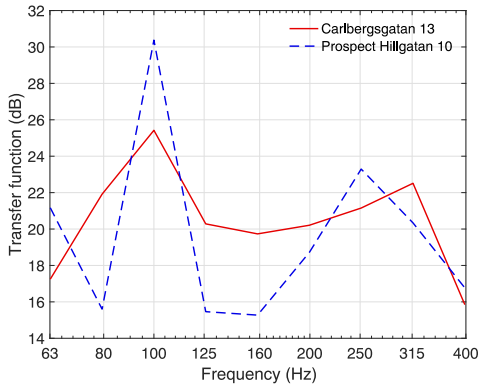

Figure 3.28: Transfer function from floor vibration to sound pressure level.

Room acoustic theory

The sound pressure level within a room can be estimated using Eq. 3.8, which provides a theoretical relationship between floor vibrations and acoustic response. This equation is applied to estimate the indoor sound pressure levels at both Carlbergsgatan 13 and Prospect Hillgatan 10.

$$L_{\mathrm{p}} = L_{\mathrm{v}} + 10\log_{10}\sigma + 10\log_{10}\frac{4S_{\mathrm{Rad}}}{A} \qquad \text{(dB)}. \tag{3.8}$$

The surface area of the interior walls and floor in the rooms (S_{Rad}) is approximately 37.5 m^2, and the room volume (V) is around 15 m^3. These values are nearly identical for both Carlbergsgatan 13 and Prospect Hillgatan 10. It is assumed that all surfaces within the room actively vibrate and contribute to noise generation. Additionally, the radiation efficiency is assumed to be $\sigma = 1$, and the reverberation time (T_{60}) is set to 0.5 s.

By substituting these parameters into Eq. 3.8, the resulting sound pressure level (L_{p}) inside the room can be calculated as follows:

$$L_{\mathrm{p}} = L_{\mathrm{v}} + 14 \qquad \text{(dB)}. \tag{3.9}$$

Based on Eq. 3.9, the estimated difference between the vibration level and the resulting sound pressure level inside the room is approximately 14 dB. However, the measured values (see Figure 3.28) indicate a larger difference, closer to 20 dB. One possible explanation for this discrepancy is that the statistical room acoustics model is not entirely valid in small basement rooms, such as those used in this study.

In particular, the Schroeder frequency for these rooms is approximately 370 Hz, which lies within the frequency range of interest (20–1000 Hz). This suggests that modal behavior may still influence the room's acoustic response, leading to increased uncertainty when applying Eq. 3.8 to estimate the sound pressure level.

3.4.10 Analysis of measurements for construction stage

To evaluate the efficiency of the applied excitation sources and their potential for model validation, vibration levels measured on the Västlänken tunnel (Kvarnberget), Gothenburg, are analyzed here.

Vibration levels recorded on the tunnel wall are presented in Figure 3.29. The results show that both excitation sources generated high vibration levels in the frequency range of interest (50–1000 Hz), with the hydraulic hammer producing significantly stronger signals, approximately 15 dB higher than the shaker between 200 and 1000 Hz. The signal-to-noise ratio is sufficiently high above 50 Hz, confirming the reliability of the measurements within this range; however, applying a band-pass filter centered around the excitation frequency of the shaker could potentially further enhance the signal-to-noise ratio.

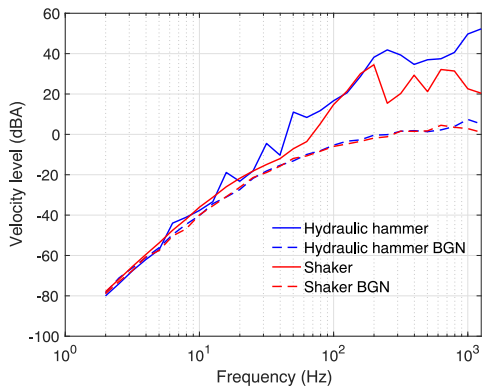

Figure 3.29: Vibration level on tunnel wall.

Despite the significant vibration levels observed at the tunnel wall, no measurable vibrations or ground-borne noise were recorded inside the house located above the tunnel, even though both structures are founded on the same bedrock. This suggests substantial attenuation along the transmission path, which could be due to energy loss in the rough concrete layer of the track, weak coupling between the concrete wall and the bedrock, weak coupling between the bedrock and the building foundation,

or a combination of these factors. Consequently, the vibration levels recorded at the house were insufficient for use in refining the developed model or for estimating a meaningful transfer function. The analysis was therefore limited to comparing the relative excitation strength of the shaker and hammer at the tunnel wall.

In summary, both excitation methods provided vibration levels suitable for analysis at the tunnel wall, fulfilling the requirements of the measurement method. However, the hydraulic hammer is generally preferable due to its ability to generate higher vibration levels and its cost-effectiveness, making it a more practical option for field measurements. Although no measurable signals were detected inside the building above the tunnel in this specific case, the stronger excitation from the hammer increases the likelihood of capturing usable signals at greater distances in future applications.

CHAPTER 4

Numerical analysis

In this chapter, numerical simulations are performed to analyze wave propagation in underground in bedrock. The study primarily focuses on two key aspects: 1) The effect of the tunnel itself on wave propagation (commonly referred to as the tunnel shielding effect). 2) The impact of cracked zones in the bedrock on wave transmission. Both 2D and 3D numerical models are developed to assess how vibrations travel from the tunnel to the ground surface, with particular attention to wave behavior at different locations, including the tunnel floor, tunnel walls, and ground surface.

4.1 Tunnel shielding effect

The finite element method (FEM) is used to simulate wave propagation and the resulting vibration amplitudes in a lightly damped elastic medium representative of Swedish bedrock, under unit load excitation. The response is evaluated across a frequency range up to 1 kHz. To capture different spatial effects, both 2D and 3D tunnel configurations are modeled, considering half-space and full-space domains, as illustrated in Figure 4.1.

The simulated bedrock is characterized as a homogeneous, isotropic elastic material, excluding the effects of cracks or inhomogeneities. The material properties used

in the model are: Young's modulus of 50 GPa, density of 2400 kg/m^3, Poisson's ratio of 0.3, and a loss factor of 0.008. The simulations are conducted using the Structural Mechanics Module of COMSOL Multiphysics, the Solid Mechanics interface in the frequency domain, to evaluate the velocity response to a unit excitation force.

To simulate an unbounded domain and avoid wave reflections at model boundaries, low-reflection boundary conditions are applied using an impedance matching approach. The boundary impedance is defined as $\rho(c_p + c_s)/2$, where c_p and c_s represent the P-wave and S-wave speeds, respectively, and ρ is the density of the bedrock.

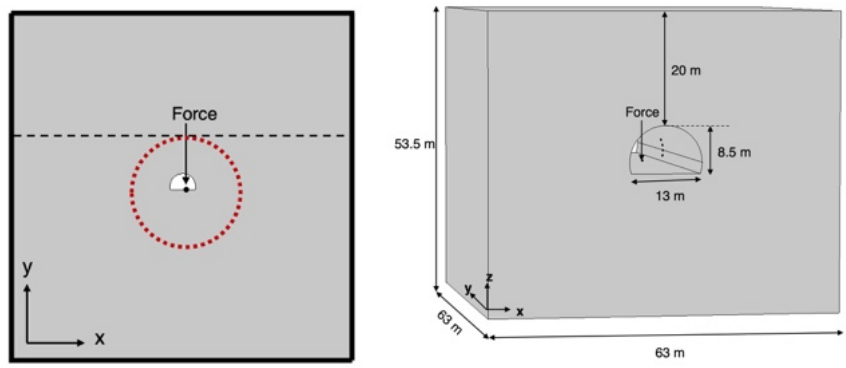

(a) (b)

Figure 4.1: Geometrical layouts of the study: (a) 2D model where the dashed line indicates the free surface in the half-space case, (b) 3D model.

Results

This section presents selected results from the 2D finite element simulations, focusing on wave directivity, vibration amplitudes at the ground surface, and vibration responses on the tunnel wall.

Figure 4.2 illustrates the radial directivity of vibration magnitude levels from the 2D finite element simulations, shown for six 1/3-octave bands representing low (10 and 20 Hz), medium (80, 160, and 250 Hz), and high (1 kHz) frequencies. The results compare full-space and half-space tunnel configurations.

For the full-space case, vibration levels increase beneath the tunnel, suggesting energy concentration below the structure. A reduction in vibration levels is observed

above the tunnel, although this effect is not consistent in all directions, for example the area directly above the tunnel shows less reduction.

Below the tunnel, results from the full- and half-space models are similar. However, above the tunnel, where wave interaction and Rayleigh wave (R-wave) formation become significant, noticeable differences emerge between the two cases. At high frequencies (e.g., 1 kHz), the half-space model shows large directional fluctuations without a consistent attenuation pattern above the tunnel. Nonetheless, vibration levels above the tunnel remain generally lower than those below, indicating that the wave energy is directed downward.

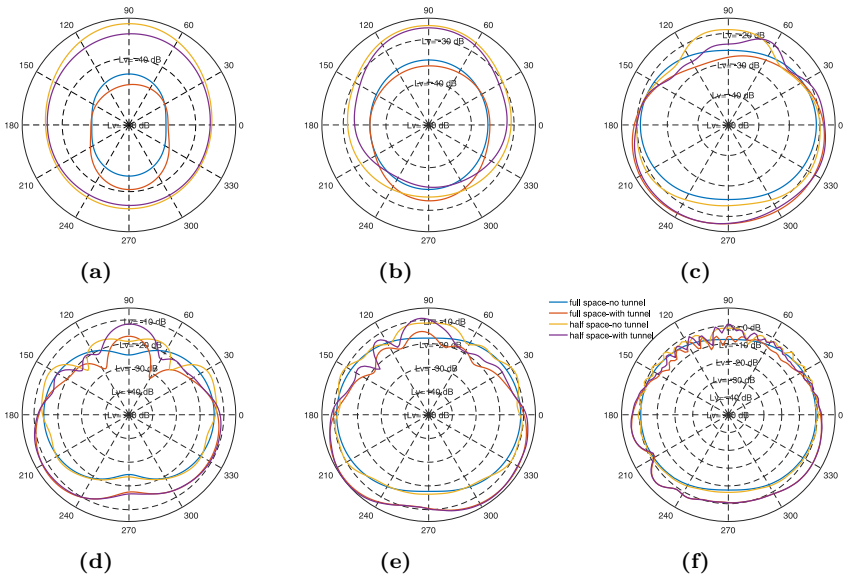

Figure 4.2: Directivity: (a) $f = 10$ Hz, (b) $f = 20$ Hz, (c) $f = 80$ Hz, (d) $f = 160$ Hz, (e) $f = 250$ Hz, (f) $f = 1$ kHz.

Vibration responses in the y-direction at the ground surface are analyzed and presented in Figure 4.3, covering a range of frequencies from low to high. Results are shown for simulations both with and without the tunnel to illustrate the influence of tunnel presence on surface vibrations.

At low frequencies (e.g., 10 Hz), a clear distance-dependent attenuation pattern is observed. As the frequency increases, interference effects between different wave types (e.g., P- and S-waves) become more pronounced, resulting in fluctuations in vibration levels along the surface. These fluctuations are particularly strong in

the mid-frequency range, where the S-wave wavelength becomes comparable to the tunnel width. They are even more pronounced at high frequencies, when the P-wave wavelength becomes smaller than the tunnel width.

Overall, the presence of the tunnel leads to noticeably lower surface vibration levels compared to the no-tunnel case, highlighting the tunnel shielding effect. This reduction is relatively small at low frequencies but becomes more significant at higher frequencies. In general, the vibration levels in the shielded case are about 4–10 dB lower, although local variations due to wave interference are present. Additionally, the asymmetry in vibration patterns is clearly visible, resulting from the asymmetric position of the excitation force.

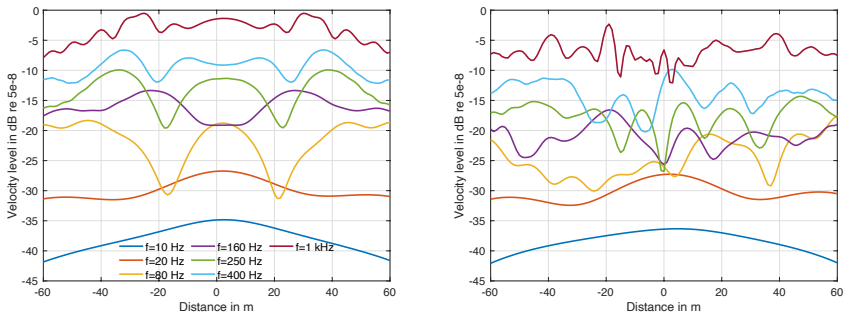

(a) (b)

Figure 4.3: Velocity level perpendicular to the ground surface: (a) half-space without the tunnel, (b) half-space with the tunnel. The legend shows the 1/3 octave center frequency in Hz.

Figure 4.4 presents the simulated vibration responses at receiver positions along the tunnel floor and tunnel wall. The tunnel floor response is evaluated in the y-direction, while the tunnel wall response is calculated in both the x- and y-directions.

In Figure 4.4(a), the vibration levels along the tunnel wall are shown for both directions. Figure 4.4(b) displays the same data, but the results are normalized to the y-direction velocity on the tunnel floor at a reference point 1 m from the excitation source, enabling a clearer comparison of relative attenuation patterns.

As expected, the vibration level on the tunnel floor decreases with increasing distance from the point of excitation due to geometric spreading and material damping. For the tunnel wall, the y-direction vibration level also declines with elevation (i.e., increasing height above the tunnel floor), indicating a vertical attenuation trend. In contrast, the x-direction vibration level remains relatively constant along the

wall, with some deviation observed particularly in the mid-frequency range (approximately 50–200 Hz), where wave mode interactions and structural resonances may become more significant.

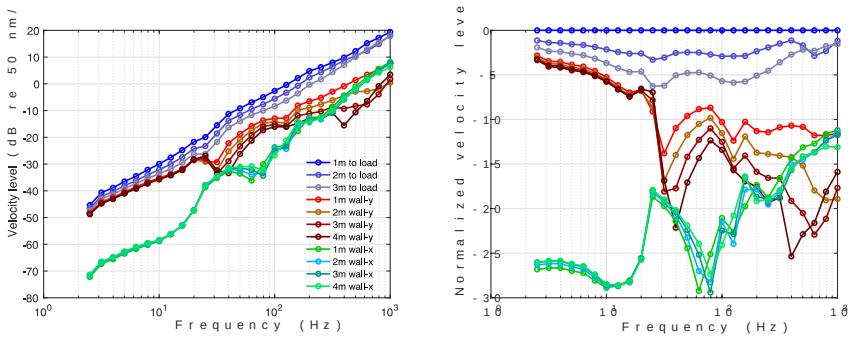

(a) (b)

Figure 4.4: Velocity level in 1/3 octave bands in the tunnel: (a) velocity level on the floor in the y-direction and on the tunnel wall in x and y-direction, (b) normalized velocity level on the floor in the y-direction and on the tunnel wall in x and y-direction.

Overall, the numerical results highlight the importance of selecting an appropriate reference position when evaluating vibration levels. The findings show a notable reduction in vertical vibration velocity when comparing the tunnel floor to the tunnel wall, especially at frequencies above 20 Hz. This attenuation is even more pronounced in the horizontal direction. A more detailed analysis of these results is presented in PartII.

4.2 Effect of cracked zone

In this section, the finite element method (FEM) is employed to simulate the influence of cracked zones in bedrock on vibration levels at the ground surface. In reality, geological cracks and fracture networks exhibit significant variability in orientation, length, width, and spatial distribution, making them complex to model directly in numerical simulations. Accurately capturing this heterogeneity would require highly detailed geological surveys and computationally expensive 3D meshing, which is often impractical and time-consuming. To address this challenge, a simplified yet representative model is adopted: a vertically oriented cracked zone is introduced in the geometry and is assigned effective material properties that differ from those of

the surrounding bedrock. While idealized, this approach enables the investigation of how a mechanically weakened region, such as a fracture or damaged rock mass, affects the propagation of vibrations toward the ground surface.

The surrounding bedrock is modeled as a linear elastic, homogeneous, and isotropic medium, with properties representative of typical Swedish bedrock: Young's modulus 50 GPa, density 2400 kg/m^3, Poisson's ratio 0.25, and loss factor 0.01. Simulations are carried out in the frequency domain using the Solid Mechanics interface of the Structural Mechanics Module in COMSOL Multiphysics. A unit point load is applied underground to mimic a localized vibration source. To ensure numerical accuracy, mesh size is adapted to maintain a minimum of six nodes per wavelength across the frequency range of interest.

Receiver points are placed on both sides of the cracked zone at 1 m intervals to capture the scattering of vibrations on ground surface (red dots in Figure 4.5).

The model is enclosed by Perfectly Matched Layers. To evaluate the performance of boundary conditions in wave propagation modeling, both low-reflection and Perfectly Matched Layer (PML) approaches were implemented and compared in a 2D domain of 80 m $\times$ 60 m. The low-reflection boundary used an impedance-matching strategy, with impedance defined as $\rho(c_p + c_s)/2$, while the PML had a thickness of 15 m applied on all sides. In frequency-domain simulations, PML performance depends on coordinate stretching, requiring only minimal physical thickness for an effective mesh. To validate the simulations, the results are compared with the analytical response of an infinite homogeneous medium to line sources, using in-plane SV-P wave solutions as described by Kausel [19]. The same material properties were used in both theoretical and simulation models for consistency.

A sensitivity analysis is performed to investigate the influence of individual cracked zone properties on the transmitted vibration. A vertical layer with a width of 2 meters is positioned 10 meters from the source (see Figure 4.5), and one parameter is varied at a time, including Young's modulus, density, damping ratio, and Poisson's ratio, while others remain fixed to bedrock values. This parametric study helps identify which properties most significantly affect vibration attenuation or amplification.

Results

Boundary condition

A comparison between PML and low-reflection boundary conditions was carried out for two different ground types: soft soil and stiff bedrock.

As shown in Figure 4.6(a), for stiff bedrock with a Young's modulus of 50 GPa, density of 2400 kg/m^3, Poisson's ratio of 0.3, and a low loss factor of 0.008, the low-reflection boundary resulted in noticeable deviations from the theoretical response.

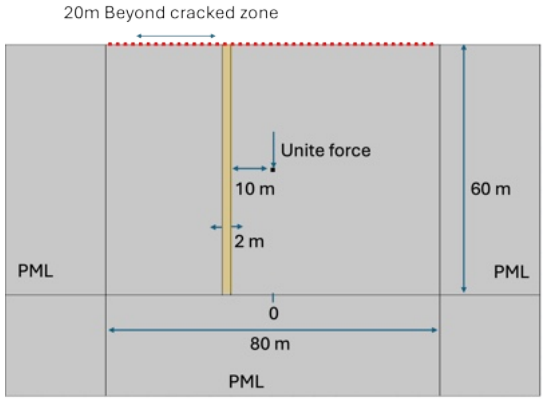

Figure 4.5: Model geometry for cracked zone configuration.

In contrast, the PML boundary closely followed the theoretical curve, demonstrating better performance in minimizing artificial reflections.

For soft soil, with a Young's modulus of 500 MPa, density of 1800 kg/m^3, Poisson's ratio of 0.3, and a higher loss factor of 0.1, both boundary conditions performed well. As shown in Figure 4.6(b), the results from both the low-reflection and PML boundaries were in good agreement with the theoretical response. This suggests that for softer and more damped materials, the difference in performance between the two boundary types becomes negligible.

Overall, the results suggest that while the low-reflection boundary may be sufficient for loose soil, the PML boundary provides more accurate and reliable results across different soil types, particularly in stiff bedrock environments.

Sensitivity analysis of cracked zone properties

First, the vibration velocity level at the ground surface is computed without the presence of a cracked zone, serving as a reference case for comparison. To evaluate the effect of the cracked zone, receivers are placed beyond and at the source sides of the intended cracked zone location. Since vibration levels can fluctuate significantly between closely spaced receivers, spatial averaging is applied to obtain representative values. Here, vibration levels are averaged over a 20 m distance beyond the cracked zone, with receivers spaced every 1 m (see Figure 4.5). The resulting plots present the difference in vibration levels between the cracked and no-cracked zone cases for each simulation scenario. Changing parameters values are chosen to be represent a weaker area in bedrock.

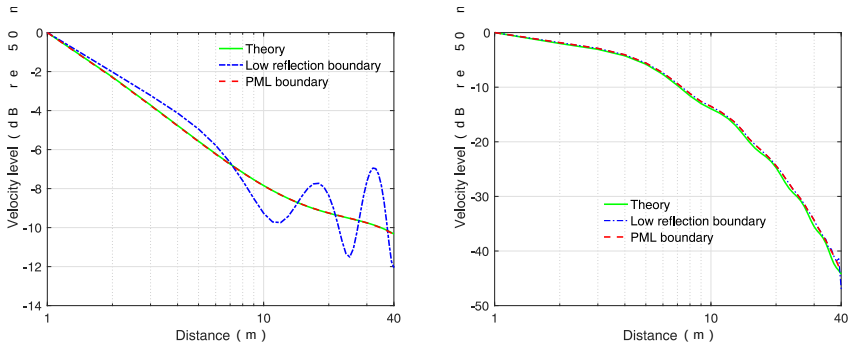

Figure 4.6: Comparison of boundary conditions at 100 Hz. (a) in stiff bedrock, (b) in soft soil.

Figure 4.7 illustrates the impact of different material parameters within the cracked zone on ground surface vibration levels, beyond the cracked zone. Each subfigure isolates a single property variation: Young's modulus (a), density (b), damping (c), and Poisson's ratio (d), while keeping the others equal to those of the surrounding intact bedrock.

For all cases, reducing the stiffness or adding higher damping of the cracked zone leads to noticeable vibration attenuation, indicating, as expected, that cracked zone with weaker mechanical properties reduce wave transmission. Among the parameters, Poisson's ratio has the least influence, showing almost no difference across the frequency range, consistent with its relatively minor role in controlling wave propagation in isotropic elastic media.

In contrast, both density and damping ratio show significant effects, particularly in the high-frequency range (300–1000 Hz). Depending on the value assigned, the vibration level can be reduced by up to 10 dB. This behavior is expected, as higher damping increases energy dissipation, and lower density leads to impedance mismatch, both contributing to greater reflection and less transmitted energy.

Young's modulus also influences the results, especially above 10 Hz. A lower modulus results in greater attenuation, consistent with slower wave speeds and reduced stiffness. However, a local peak appears around 100 Hz at both Young's modulus. This may be due to resonance effects, wave interference or conversion mode within the cracked zone.

A more detailed analysis related to the effect of the cracked zone is presented in Paper D.

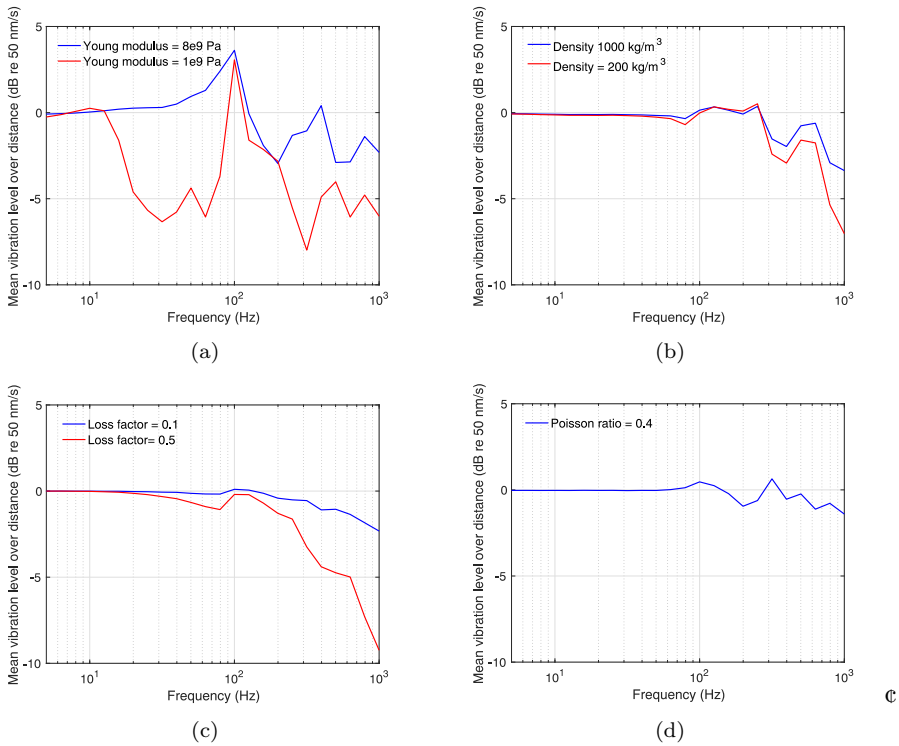

Figure 4.7: Comparison of vibration responses on the ground surface due to variations in cracked zone material properties. (a) effect of Young's modulus, (b) effect of density, (c) effect of damping ratio (loss factor), (d) effect of Poisson's ratio.

CHAPTER 5

Application of the model

The Swedish Transport Administration (Trafikverket) is currently in the early stages of planning a new tunnel between Borås and Gothenburg. A critical aspect of this planning process is identifying the most suitable location for the tunnel while minimizing its environmental impact, particularly concerning ground-borne noise. The developed ground borne noise prediction model is applied here to evaluate the risk areas on the ground based on the depth of the tunnel, determining where noise levels may exceed limitation values.

Method

Since the project is in its early phase and only limited information is available, the focus of the study is on the Location Stage, which is designed for use during the early phases of project development when limited data are available. By employing simplified and generalized input parameters, the model provides single-number results that offer a preliminary overview of expected noise levels across potential alignment options.

Due to the lack of detailed site-specific data, conservative assumptions are made for the input parameters. The train speeds are set to 250 km/h for passenger trains and 120 km/h for freight trains. The ground is assumed to be crack-free bedrock

(wave speed 5,000 m/s). A strong building foundation is assumed, meaning that vibration energy is fully transferred from the ground into the structure. The room is assumed to be normally furnished with floor surface $S = 10$ m^2 and located in a basement.

To estimate noise levels, different tunnel depths and distances from the tunnel are analyzed (Eq 5.1) to identify areas most affected by vibrations.

$$\Delta L_{\mathrm{g}} = -10 \log_{10} \frac{R}{R_{\mathrm{ref}}} + 10 \log_{10} \left(e^{-2\pi f \eta (R - R_{\mathrm{ref}})/c_{\mathrm{p}}} \right), \tag{5.1}$$

where ΔL_{g} is distance term, R is the distance from the track, R_{ref} is the reference distance used when determining the source term, η is the material loss factor, and c_{p} is the speed of the pressure wave in the ground.

According to Swedish regulation [2], the ground-borne noise limit value is 32 dBA (time-weighting Fast). The model predicts where noise levels exceed this threshold, with the results representing the mean value plus two times the estimated standard deviation (i.e., $L_{\mathrm{pAFmax}} = \langle L_{\mathrm{pAFmax}} \rangle + 2 \cdot \mathrm{STD}$). This approach helps define zones that may require mitigation measures. Additionally, the effect of material damping in the bedrock is considered, providing a more comprehensive understanding of how material damping influences ground-borne noise propagation.

Results

This section examines how material damping and tunnel depth (from tunnel floor to ground surface) influence noise levels to determine the distance from the tunnel where the limit value may be potentially exceeded in a house at ground surface without mitigation measures. The results include the maximum sound pressure level inside house plus two standard deviations (10.5 dB for passenger trains and 14 dB for freight trains [56]) to compare with the limit value.

Considering the effect of damping

Figure (5.1) shows how the material damping affects the sound pressure level at different distances from the tunnel on the ground surface for a tunnel depth of 60 m. It includes both passenger and freight trains. The y-axis represents the predicted sound pressure level in a house at ground surface above the tunnel, while the x-axis shows the distance from the tunnel center at the ground surface to the house.

As shown, the loss factor has a significant impact on the final results. With high damping ($\eta = 0.1$), the sound level inside the house stays below the limit value for all distances. However, as damping decreases, the distance where the sound level exceeds the limit value increases. For example, for freight trains (Figure 5.1b) with

$\eta = 0.001$, the distance at which the sound level surpasses the limit extends up to 1250 m.

Based on the developed model [56], if no specific information is available, it is recommended to use a loss factor of 0.01.

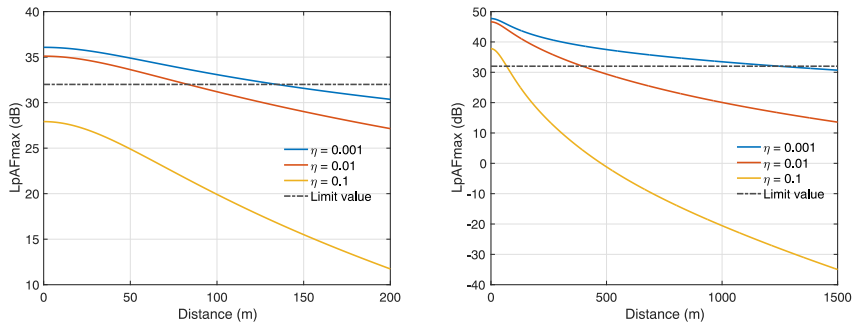

Figure 5.1: Predicted sound pressure levels inside a house on ground level at different distances for different material damping in the bedrock: (a) passenger train, (b) freight train. The tunnel depth is 60 m.

Considering the effect of tunnel depth

This section analyzes the impact of tunnel depth on the influential distance, defined as the horizontal distance on the ground surface from the tunnel centerline at which the maximum indoor sound level exceeds the limit value, for passenger and freight trains, respectively. The loss factor is selected to be 0.01.

Plots in Figure 5.2 illustrate the relationship between tunnel depth and the influential distance. For passenger trains (Figure 5.2a), the influential distance decreases from approximately 100 m at a tunnel depth of 10 m to 65 m at a depth of 80 m. In contrast, for freight trains (Figure 5.2b), the influential distance decreases only slightly, from 400 m at 10 m depth to 393 m at 80 m depth.

Discussion and conclusion

For the distance term analysis, it is assumed that trains acts as a line load. This is a conservative assumption. However, in some cases, especially with freight trains, individual wagons may be much heavier and wheel flats may be present, making the maximum level be caused by individual bogies that act like point sources. Similarly,

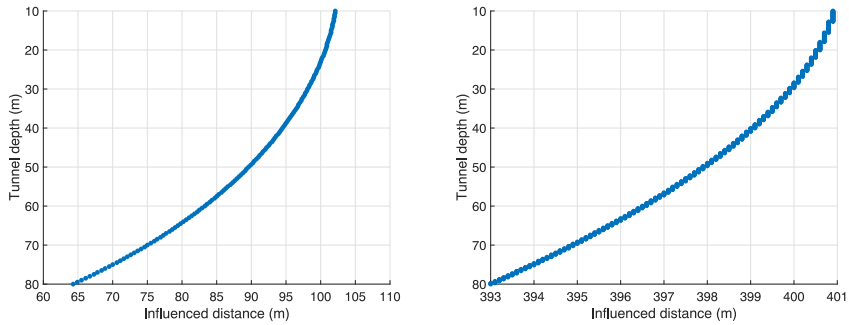

(a) (b)

Figure 5.2: Influential distance on ground surface, (a) passenger train, (b) freight train. The loss factor is set to 0.01.

for passenger trains, wheel flats and switches can sometimes make the train behave more like a point load. Since these conditions don't apply to all trains consistently, the safer and more conservative choice is to treat the train as a line load.

The loss factor has a significant impact on the influential distance at the ground surface. Therefore, having detailed information about the site properties is crucial for making accurate predictions and determining the necessary mitigation measure.

The influential distance for various common tunnel depths, 10–80 m, is estimated to be around 400 m for freight trains. For passenger trains, the influential distance is estimated to be around 100 m for shallow tunnels and about half of that for the deeper tunnels. Thus, the freight train at 120 km/h is the dimensioning case for the Göteborg-Borås railway.

The noise level estimation in this study is a conservative prediction, as the project is still in its early phase and detailed site information is not yet available.

CHAPTER 6

Summary of appended papers

Paper A: Finite element modelling of tunnel shielding in vibration measurements of ground-borne noise

This paper uses finite element modeling to analyze how a tunnel in bedrock affects the transmission of vibrations, specifically ground-borne noise. The study investigates this tunnel shielding effect by simulating wave propagation up to 1 kHz in 2D and 3D models representative of Swedish bedrock conditions. Results indicate that vibration levels differ between the tunnel floor and wall, with the tunnel generally causing reduced vibration levels above it at mid-frequencies and fluctuating levels at higher frequencies. Comparisons between 2D and 3D models show similar trends in vibration behavior and the tunnel's shielding influence on both the ground surface and directivity patterns.

Paper B: A framework in three different project stages to predict ground-borne noise of trains in railway tunnels

This paper introduces a three-stage framework for predicting ground-borne noise from trains in railway tunnels, adapting to the varying levels of information available during project development: location, planning, and construction. The proposed model incorporates a source term and correction terms for factors like train speed and distance, along with a statistical method to quantify uncertainty at each stage of the prediction. Measurements from Swedish railway tunnels and buildings were

used to develop the model, which operates using single values in early stages and frequency bands for increased accuracy at later stage. The study aims to provide a comprehensive approach for predicting and managing railway-induced ground-borne noise in nearby structures.

Paper C: Investigation of the relation between horizontal and vertical vibration levels on railway tunnel walls and at ground surface

This research investigates vibration levels from railway traffic in tunnels, specifically examining the differences between horizontal and vertical vibrations on tunnel walls and their relationship to ground surface vibrations. Through numerical simulations and field measurements in Swedish bedrock tunnels, the study reveals a frequency-dependent difference between horizontal and vertical vibration levels on tunnel walls, with the level gap decreasing from about 14 dB at 60 Hz to 0 dB at 1000 Hz. Based on this, vertical vibration is proposed as a more reliable indicator for ground-borne noise prediction. The work also explores how the presence of a tunnel and distance affect vibration propagation to the surface and introduces a correction term for converting horizontal to vertical vibration levels for similar tunnel environments.

Paper D: The effect of cracked zone in bedrock on ground-borne vibration generated by underground sources

This paper examines the impact of cracked bedrock zones on ground vibrations stemming from underground tunnels, utilizing numerical simulations in both 2D and 3D. The research evaluates how factors like the width of the cracked zone, its distance from the tunnel, and the tunnel's depth influence vibration levels at the surface. Key findings indicate that vibration attenuation beyond the cracked zone depends on frequency and width, while amplification occurs on the source side due to wave reflections. Distance from the tunnel primarily affects amplification, and deeper tunnels generally lead to less attenuation beyond the cracked zone.

Report: Ground Borne Noise Model and Methodology Description

This report presents a model and methodology specifically developed for predicting ground-borne noise in projects managed by the Swedish Transport Administration. The model is adapted to Swedish bedrock conditions based on new measurement campaigns in the Gårda tunnel in Gothenburg, as well as on existing data from the Åsa tunnel near Varberg and the Håknäs tunnel along the Bothnia Line.

The methodology is structured around three stages, reflecting the level of available information and required precision: the location stage, the planning stage, and the construction stage. The first two stages correspond to early project planning and railway design, while the third stage covers construction, when more detailed site-

specific data can be collected. The prediction framework is formulated for Swedish bedrock conditions across a frequency range of 20 Hz to 1 kHz and is based on a source term combined with several correction terms. These corrections account for factors such as train speed, distance attenuation, ground-to-building transmission, vibration transmission to various building elements, the influence of room acoustics on interior sound pressure levels, and the effects of different track treatments. In addition, statistical methods have been applied to account for uncertainties associated with each component of the model.

CHAPTER 7

Conclusions and Future Work

Conclusion

This study developed a methodology and prediction model for ground-borne noise generated by railway tunnel traffic, specifically adapted for Swedish bedrock conditions. The model integrates both numerical simulations and empirical data, with the empirical data obtained from measurements conducted in the Gårda, Åsa, and Håknäs tunnels.

The methodology is structured into three stages: the location stage, planning stage, and construction stage. In the location stage, which corresponds to the early phase of the project, the model provides a single-value prediction. At the planning stage, the parameters are refined into frequency-dependent functions, expressed in 1/3-octave bands up to 1 kHz, offering improved precision compared to the location stage. During the construction stage, site-specific measurements from the tunnel under construction can be incorporated to validate and adjust the predictions made in the planning phase, ensuring greater model reliability and accuracy.

The prediction model (in Part **??**, Report) incorporates a source term and several correction terms, including train speed, distance attenuation, ground-to-building coupling, vibration levels on different floors, and the influence of room properties on sound pressure levels within rooms. Additionally, standard deviations related to each model term have been used to estimate the uncertainty for the whole model.

In order to determine how vibration levels change with position in the tunnel, numerical analyses are conducted. The receiver positions are located along the tunnel floor and tunnel wall. As a result, from the tunnel floor to the tunnel wall, there is a clear reduction in vertical velocity above 20 Hz, and the horizontal velocity is even lower. This phenomenon can be called the tunnel shielding effect. Additionally, the importance of the vibration level in different directions is considered on the tunnel wall. If only one direction should be considered, it is proposed to use the vertical vibration level as the source term for such models since the vertical direction captures the main vibration energy and is close to the magnitude level. This study also suggests a relationship between vibration levels in the horizontal and vertical directions on the tunnel wall as a function of frequency.

The results of the cracked zone study demonstrate that the presence of a cracked region in the bedrock significantly affects vibration transmission. Vibrations are attenuated beyond the cracked zone, and this attenuation is strongly frequency-dependent. On the source side of the cracked zone, an amplification of vibration levels is observed, with increases of up to 5 dB in some cases.

Overall, the developed model and methodology fulfills the project's aim of providing a practical, adaptable, and comprehensive tool for predicting ground-borne noise from railway tunnels. It supports decision-making across two project stages (location and planning stages) and incorporates the most relevant factors influencing vibration transmission and indoor noise levels. The measurement-based approach and structured handling of uncertainty make the model suitable for applications within the Swedish Transport Administration's infrastructure projects.

Future work

The current model is developed with a focus on railway tunnels and structures founded on bedrock. Future work could expand its scope to cover additional scenarios, such as ballastless track systems or buildings equipped with vibration-dampening features. To support such extensions, further measurement campaigns would be required to maintain model reliability and accuracy across different configurations.

In addition, several model parameters and empirical relationships may require refinement as new experimental data become available. Systematically updating the model using continuous measurement data will allow it to evolve and better reflect site-specific conditions, particularly those found in Swedish infrastructure projects.

Uncertainties exist across various stages of the vibration propagation path, including the vibration source itself, transmission from tunnels to structures, ground-to-building coupling, and internal propagation within the building. These sources of variability should be more thoroughly addressed in future refinements of the model.

Additionally, collecting more measurement data, especially across different sites and conditions, will help to reduce these uncertainties and improve the model's reliability.

In this study, a simplified model was used to represent the cracked zone in bedrock, allowing for efficient numerical analysis while capturing the key effects on vibration propagation. For future work, more complex and geologically realistic models, such as those incorporating irregular crack geometries, varying orientations, and fracture networks, could be developed to better approximate real-world conditions. In addition, site-specific measurements of vibration transmission across actual cracked zones in bedrock are recommended to validate and refine the numerical model.

References

[1] Z. Xuetao, H. Jonasson, and K. Holmberg, "Source modelling of train noise-literature review and some initial measurements," 2000.

[2] Trafikverket, " Buller och vibrationer från trafik på väg och järnväg," TDOK 2014:1021, Dokumentdatum 2020-09-25, Version 3.0, Fastställt av Gäller från Ersätter Chef VO Planering 2021-01-01.

[3] R. Hood, R. Greer, M. Breslin, and P. Williams, "The calculation and assessment of ground-borne noise and perceptible vibration from trains in tunnels," *Journal of sound and vibration*, vol. 193, no. 1, pp. 215–225, 1996.

[4] ISO, "Mechanical vibration – Ground-borne noise and vibration arising from rail systems – Part 1: General guidance," ISO 14837-1, 2005.

[5] B. Möller, R. Larsson, P.-E. Bengtsson, and L. Moritz, *Geodynamik i praktiken*, 2000.

[6] L. Hall, "Simulations and analyses of train-induced ground vibrations in finite element models," *Soil Dynamics and Earthquake Engineering*, vol. 23, no. 5, pp. 403–413, 2003.

[7] A. Colaço, P. A. Costa, and D. P. Connolly, "The influence of train properties on railway ground vibrations," *Structure and Infrastructure Engineering*, vol. 12, no. 5, pp. 517–534, 2016.

[8] L. Kurzweil, "Ground-borne noise and vibration from underground rail systems," *Journal of Sound and Vibration*, vol. 66, no. 3, pp. 363–370, 1979.

[9] Y. Chi, H. Xiao, M. M. Nadakatti, Z. Zhang, and Y. Wang, "Impact of speed and axle load on the static and dynamic mechanical behavior of the ballast bed laying under sleeper pads," *Construction and Building Materials*, vol. 423, p. 135 906, 2024.

[10] A. Mirza, A. Frid, and J. Nielsen, "Reduction of train induced ground vibration by vehicle design," in *Noise and Vibration Mitigation for Rail Transportation Systems: Proceedings of the 11th International Workshop on Railway Noise, Uddevalla, Sweden, 9–13 September 2013*, Springer, 2015, pp. 523–530.

[11] H. J. Saurenman, R. L. Shipley, G. P. Wilson, I. Wilson, D. Cather, *et al.*, "In-service performance and costs of methods to control urban rail system noise," United States. Department of Transportation. Urban Mass Transportation ..., Tech. Rep., 1979.

[12] M. Kazemian, F. Astaraki, A. Dosst, M. Akbarivarmayiar, M. M. Rad, and S. Fischer, "Effects of wheel surface defects on ground borne vibration," *Acta Polytech. Hung*, vol. 19, pp. 129–141, 2022.

[13] M. Bačić, L. Librić, D. J. Kaćunić, and M. S. Kovačević, "The usefulness of seismic surveys for geotechnical engineering in karst: Some practical examples," *Geosciences*, vol. 10, no. 10, p. 406, 2020.

[14] J. Achenbach, *Wave propagation in elastic solids*. Elsevier, 2012.

[15] E. Ungar and E. Bender, "Vibrations produced in buildings by passage of subway trains; parameter estimation for preliminary design," Tech. Rep., 1975.

[16] R. D. Woods and L. P. Jedele, "Energy—attenuation relationships from construction vibrations," in *Vibration problems in geotechnical engineering*, ASCE, 1985, pp. 187–202.

[17] T. G. Gutowski and C. L. Dym, "Propagation of ground vibration: A review," *Journal of Sound and Vibration*, vol. 49, no. 2, pp. 179–193, 1976.

[18] E. Taniguchi and K. Sawada, "Attenuation with distance of traffic-induced vibrations," *Soils and foundations*, vol. 19, no. 2, pp. 15–28, 1979.

[19] E. Kausel, *Fundamental solutions in elastodynamics: a compendium*. Cambridge University Press, 2006.

[20] T. Lay, *Quantitative seismology*, 2003.

[21] A. Eitzenberger, "Wave propagation in rock and the influence of discontinuities," PhD thesis, Luleå University of Technology, 2012.

[22] L. J. Pyrak-Nolte, L. R. Myer, and N. G. Cook, "Anisotropy in seismic velocities and amplitudes from multiple parallel fractures," *Journal of Geophysical Research: Solid Earth*, vol. 95, no. B7, pp. 11 345–11 358, 1990.

[23] ——, "Transmission of seismic waves across single natural fractures," *Journal of Geophysical Research: Solid Earth*, vol. 95, no. B6, pp. 8617–8638, 1990.

[24] M. Schoenberg, "Elastic wave behavior across linear slip interfaces," *The Journal of the Acoustical Society of America*, vol. 68, no. 5, pp. 1516–1521, 1980.

[25] J. A. Hudson, "Wave speeds and attenuation of elastic waves in material containing cracks," *Geophysical Journal International*, vol. 64, no. 1, pp. 133–150, 1981.

[26] D. A. T. Carl E. Hanson and L. D. Meister, *Transit noise and vibration impact assessment*. US Department of Transportation, Federal Transit Administration, 2006.

[27] M. Villot, S. Bailhache, C. Guigou, and P. Jean, "Prediction of railway induced vibration and ground borne noise exposure in building and associated annoyance," in *Noise and Vibration Mitigation for Rail Transportation Systems*, Springer, 2015, pp. 289–296.

[28] S. OCH and P. RAPPORTER, "Skadlig inverkan av vibrationer,"

[29] A. Quagliata, M. Ahearn, E. Boeker, C. Roof, L. Meister, and H. Singleton, "Transit noise and vibration impact assessment manual," Tech. Rep., 2018.

[30] P. J. Remington, L. G. Kurzweil, and D. A. Towers, "Low-frequency noise and vibration from trains," *Transportation noise reference book*, 1987.

[31] J. Melke, "Noise and vibration from underground railway lines: Proposals for a prediction procedure," *Journal of Sound and Vibration*, vol. 120, no. 2, pp. 391–406, 1988.

[32] M. Villot, P. Jean, L. Grau, and S. Bailhache, "Predicting railway-induced ground-borne noise from the vibration of radiating building elements using power-based building acoustics theory," *International Journal of Rail Transportation*, vol. 6, no. 1, pp. 38–54, 2018.

[33] C. Soize, "A comprehensive overview of a non-parametric probabilistic approach of model uncertainties for predictive models in structural dynamics," *Journal of sound and vibration*, vol. 288, no. 3, pp. 623–652, 2005.

[34] G. Paneiro, F. Durão, M. C. e Silva, and P. F. Neves, "Prediction of ground vibration amplitudes due to urban railway traffic using quantitative and qualitative field data," *Transportation Research Part D: Transport and Environment*, vol. 40, pp. 1–13, 2015.

[35] J. Forrest and H. Hunt, "A three-dimensional tunnel model for calculation of train-induced ground vibration," *Journal of sound and vibration*, vol. 294, no. 4-5, pp. 678–705, 2006.

[36] Z. Li, Y. Cao, M. Ma, and Q. Xiang, "Prediction of ground-borne vibration from random traffic flow and road roughness: Theoretical model and experimental validation," *Engineering Structures*, vol. 285, p. 116 060, 2023.

[37] P. Fiala, G. Degrande, and F. Augusztinovicz, "Numerical modelling of ground-borne noise and vibration in buildings due to surface rail traffic," *Journal of Sound and Vibration*, vol. 301, no. 3-5, pp. 718–738, 2007.

[38] P. Jean, "A 2.75 d model for the prediction of noise inside buildings due to train traffic," *Acta Acustica united with Acustica*, vol. 104, no. 6, pp. 1009–1018, 2018.

[39] W. Liu, C. Li, L. Ma, and L. Du, "A frequency-domain formulation for predicting ground-borne vibration induced by underground train on curved track," *Journal of Sound and Vibration*, vol. 549, p. 117 578, 2023.

[40] N. Pontani, L. Martinelli, M. Acquati, and C. Jommi, "A numerical assessment of variable saturation of the upper layers on the ground borne vibrations from underground trains: A case history," *Transportation Geotechnics*, vol. 40, p. 100 981, 2023.

[41] K. Kuo, H. Verbraken, G. Degrande, and G. Lombaert, "Hybrid predictions of railway induced ground vibration using a combination of experimental measurements and numerical modelling," *Journal of Sound and Vibration*, vol. 373, pp. 263–284, 2016.

[42] R. Arcos, P. J. Soares, P. A. Costa, and L. Godinho, "An experimental/numerical hybrid methodology for the prediction of railway-induced ground-borne vibration on buildings to be constructed close to existing railway infrastructures: Numerical validation and parametric study," *Soil Dynamics and Earthquake Engineering*, vol. 150, p. 106 888, 2021.

[43] Z. Li, M. Ma, M. Li, M. Zhou, and L. Xu, "Hybrid method combining numerical modelling and experimental measurements for predicting ground-borne vibrations induced by underground trains," *Soil Dynamics and Earthquake Engineering*, vol. 187, p. 108 959, 2024.

[44] J. Manning, R. Cann, J. Fredberg, *et al.*, "Prediction and control of rail transit noise and vibration-a state-of-the-art assessment," United States. Urban Mass Transportation Administration, Tech. Rep., 1974.

[45] G. Wilson, "Ground-borne vibration levels from rock and earth base subways," *Report. Wilson Ihrig & Associates Inc., Oakland, California, US*, 1971.

[46] RENVIB II Final Report Phase 1 and Phase 2; ERRI Utrecht, 2000.

[47] V. Jurdic, O. Bewes, R. Greer, and T. Marshall, "Developing prediction model for ground-borne noise and vibration from high speed trains running at speeds in excess of 300km/h," in *The 21st International Congress on Sound and Vibration (ICSV)*, Beijing/China, 2014.

[48] R. Greer, "Methods for predicting groundborne noise and vibration from trains in tunnels," in *Local Authority Railway Impact Forum (LARIF)*, 1999.

[49] J. T. Nelson, H. J. Saurenman, I. Wilson, *et al.*, "State-of-the-art review: Prediction and control of groundborne noise and vibration from rail transit trains," 1983.

[50] M. Källman, "Mätrapport - Långtidsmätning av vibrationer i Åsatunneln," ÅF Infrastructure AB, Tech. Rep., 2020.

[51] T. Odebrant, "Höghastighetsprojektet. Stomljud. Slutrapport," PM10. Uppdragsnummer 552777. Trafikverket, Tech. Rep., 2010.

[52] Trafikverket, " Banunderbyggnad i tunnlar för ballastspår och ballastfria spårkonstruktioner," Document, Trafikverket, 2020.

[53] J. Nordström, "Empirical prediction of ground-borne vibration from railway systems; validating the hs2 model in sweden, west coast," 2023.

[54] I. BIPM, I. Ifcc, I. Iso, and O. Iupap, "Evaluation of measurement data—guide to the expression of uncertainty in measurement, jcgm 100: 2008 gum 1995 with minor corrections," *Joint Committee for Guides in Metrology*, 2008.

[55] P. Karantonis and C. Weber, "Use of iso measurement uncertainty guidelines to determine uncertainties in noise & vibration predictions and design risks," *Proceedings of ACOUSTICS, Proceedings of ACOUSTICS, Brisbane, Australia*, pp. 1–9, 2016.

[56] F. Dashti, *A ground-borne noise prediction model for railway traffic in tunnels in bedrock*. Chalmers Tekniska Hogskola (Sweden), 2023.